https://doi.org/10.5194/acp-2020-952
Preprint. Discussion started: 13 November 2020

Atmospheric Chemistry and Physics Discussions

3D simulations of tropospheric ozone depletion events using WRF-Chem

Maximilian Herrmann [1], Holger Sihler [2,3], Thomas Wagner [2,3], Ulrich Platt [3,4], and Eva Gutheil [1,4]

[1]Interdisciplinary Center for Scientific Computing, Heidelberg University, Heidelberg, Germany
[2]Max-Planck Institute for Chemistry, Mainz, Germany
[3]Institute of Environmental Physics, Heidelberg University, Heidelberg, Germany
[4]Heidelberg Center for the Environment, Heidelberg University, Heidelberg, Germany

Correspondence: M. Herrmann (maximilian.herrmann@iwr.uni-heidelberg.de)

Abstract. Tropospheric bromine release and ozone depletion events (ODEs) as they commonly occur in the Arctic spring are studied using the regional software WRF-Chem. For this purpose, the MOZART-MOSAIC chemical reaction mechanism is extended by bromine and chlorine reactions as well as an emission mechanism for reactive bromine via heterogeneous reactions on ice and snow surfaces. The simulation domain covers an area of 5,040 km x 4,960 km, centered north of Utqiaġvik (formerly Barrow), Alaska, and the time interval from February through May, 2009. Several simulations for different strengths of the bromine emission are conducted and evaluated by comparison with in-situ and ozone-sonde measurements of ozone mixing ratios as well as by comparison with tropospheric BrO vertical column densities (VCDs) from the Global Ozone Monitoring Experiment–2 (GOME-2) satellite instrument. The base bromine emission scheme includes the direct emission of bromine due to bromide oxidation by ozone through the reactive surface ratio β of the ice/snow surface relative to a flat surface. Results of simulations with $\beta = 1.0$ agree well with the observations, however, a value of 1.5 performs somewhat better. The bromine emission due to bromide oxidation by ozone is found to be important to provide an initial seed for the bromine explosion. Consideration of halogen chemistry substantially improves the prediction of the ozone mixing ratio with respect to the observations. Meteorological nudging is found to be essential for a good prediction of ODEs over the three months period.

1 Introduction

Ozone is an important constituent of the troposphere due to its high oxidation potential. In the Arctic troposphere, ozone mainly originates from transport and photo-chemical reactions involving nitrogen oxides and volatile organic compounds, resulting in a background mixing ratio of 30 to 50 nmol/mol (ppb). During polar spring, so-called tropospheric ozone depletion events (ODEs) are regularly observed, in which ozone mixing ratios in the boundary layer drop to almost zero levels coinciding with a surge in reactive bromine levels on a time scale of hours to days (e.g. Oltmans, 1981; Bottenheim et al., 1986; Barrie et al., 1988; Hausmann and Platt, 1994; Wagner and Platt, 1998; Frieß et al., 2004; Wagner et al., 2007; Helmig et al., 2012; Halfacre et al., 2014). ODEs strongly shorten the lifetime of ozone and organic gases, they cause the removal and deposition of mercury as well as the transport of reactive bromine into the free troposphere. During an ODE, ozone is most likely destroyed

https://doi.org/10.5194/acp-2020-952
Preprint. Discussion started: 13 November 2020


Atmospheric Chemistry and Physics Discussions

by Br atoms in the catalytic reaction cycle (e.g. Barrie et al., 1988)

$$\mathrm{Br} + \mathrm{O_3} \rightarrow \mathrm{BrO} + \mathrm{O_2} \tag{R1}$$

$$\mathrm{BrO} + \mathrm{BrO} \rightarrow \begin{cases} 2\,\mathrm{Br} + \mathrm{O_2} \\ \mathrm{Br_2} + \mathrm{O_2} \end{cases} \tag{R2}$$

$$\mathrm{Br_2} + h\nu \rightarrow 2\mathrm{Br}, \tag{R3}$$

resulting in the net reaction

$$2\mathrm{O_3} \rightarrow 3\mathrm{O_2}. \tag{R4}$$

The rate-limiting reaction in this cycle is usually the BrO self-reaction (R2) with a reaction rate that is quadratic in the BrO concentration. The source of the reactive bromine is thought to be sea salt, i.e. aerosol, which deposits on the ice (Fan and Jacob, 1992; McConnell et al., 1992; Platt and Janssen, 1995; Simpson et al., 2015). However, it is not fully understood how the salt bromide is oxidized and how the reactive bromine is released into the air. The most widely accepted emission mechanism is autocatalytic and termed "bromine explosion" (Platt and Janssen, 1995; Platt and Lehrer, 1997; Wennberg, 1999), which consists of the reactions (R1), (R3), and the following two reactions (R5) and (R6)

$$\mathrm{BrO} + \mathrm{HO_2} \rightarrow \mathrm{HOBr} + \mathrm{O_2} \tag{R5}$$

$$\mathrm{HOBr} + \mathrm{H^+} + \mathrm{Br^-} \xrightarrow{\mathrm{aq}} \mathrm{Br_2} + \mathrm{H_2O} \tag{R6}$$

where $\xrightarrow{\mathrm{aq}}$ denotes a heterogeneous reaction, i.e. a reaction involving gaseous components (HOBr) and liquid phase components ($\mathrm{H^+}$ and $\mathrm{Br^-}$). The concentration of atomic gas-phase bromine doubles in each reaction cycle as can be seen in the following net reaction

$$\mathrm{Br} + \mathrm{Br^-} + \mathrm{H^+} + \mathrm{O_3} + \mathrm{HO_2} \rightarrow 2\mathrm{Br} + 2\mathrm{O_2} + \mathrm{H_2O}. \tag{R7}$$

Since $\mathrm{H^+}$ ions are consumed, it implies the need for acidic solutions for this reaction to occur, and a pH of at most 6.5 is suggested by Fickert et al. (1999) for this reaction to efficiently occur.

Other pathways to activate bromide were suggested, involving nitrogen oxides

$$\mathrm{BrO} + \mathrm{NO_2} + \mathrm{M} \rightarrow \mathrm{BrONO_2} + \mathrm{M} \tag{R8}$$

https://doi.org/10.5194/acp-2020-952
Preprint. Discussion started: 13 November 2020

Atmospheric Chemistry and Physics Discussions

$$BrONO_2 + Br^- \xrightarrow{aq} Br_2 + NO_3^-, \quad \text{(R9)}$$

as well as a direct emission due to bromide oxidation by ozone (e.g. Oum et al., 1998; Artiglia et al., 2017), which are likely to need sunlight to efficiently occur (Pratt et al., 2013)

$$O_3 + 2Br^- + 2H^+ \xrightarrow{aq} Br_2 + H_2O + O_2. \quad \text{(R10)}$$

In the following discussion, the term bromine explosion mechanism includes the original reactions (R1), (R3), (R5), and (R6) as well as reaction (R9), which also generates two bromine atoms out of one gas-phase bromine atom and represents an extended bromine explosion mechanism. Reaction (R10) is considered independently of this terminology as bromide oxidation due to ozone.

A further Br_2 release mechanism initiated by a reaction of the hydroxyl radical OH with bromide inside the surface layer was suggested (Sjostedt and Abbatt, 2008; Pratt et al., 2013), this was also found in a laboratory study (Halfacre et al., 2019). The release mechanism may be summarized in the net reaction

$$OH + 2Br^- + H^+ \xrightarrow{aq} Br_2 + H_2O. \quad \text{(R11)}$$

A consequence of the reduced ozone levels during an ODE is that reactions of reactive bromine with OH or certain organic species producing chemically inert HBr are favored (essentially reactive bromine is returned to the bromide reservoir), e.g.

$$Br + CH_2O + O_2 \rightarrow HBr + CO + HO_2. \quad \text{(R12)}$$

HBr then deposits into the ground or onto aerosols, ultimately terminating the ODE. Chlorine and iodine play a smaller role for the occurence of ODEs. The reaction of methane with chlorine atoms quickly produces chemically inert HCl. Since Cl-atoms react with CH_4 (while Br- and I-atoms do not) and due to the large abundance of methane in the atmosphere, chlorine explosions cannot occur in the atmosphere. The iodine concentration (I^- and IO_3^-) is approximately twenty times smaller than bromide in seawater (Luther et al., 1988; Grebel et al., 2010), which is likely the reason why detectable amounts of gaseous iodine were rarely found in the Arctic and the Antarctic (Saiz-Lopez et al., 2007; Atkinson et al., 2012; Zielcke, 2015; Raso et al., 2017). Both iodine and chlorine, however, still may play a role due to interhalogen reactions

$$BrO + XO \rightarrow BrX + O_2 \quad \text{(R13)}$$

$$BrX + h\nu \rightarrow Br + X, \quad \text{(R14)}$$

with X = Cl or I, that occur faster by an order of magnitude (Atkinson et al., 2007) than the BrO self reaction (R2).

Similarly, chloride can speed up bromine activation (Simpson et al., 2007a)

$$HOBr_{aq} + H^+ + Cl^- \xrightarrow{aq} BrCl + H_2O, \quad \text{(R15)}$$

https://doi.org/10.5194/acp-2020-952
Preprint. Discussion started: 13 November 2020


Atmospheric Chemistry and Physics Discussions

and aqueous $BrCl$ can further be converted into Br_2

$$BrCl + Br^- \xrightarrow{aq} Br_2 + Cl^-. \quad \text{(R16)}$$

ODEs are observed mostly in the polar spring. During winter, radical bromine chemistry cannot occur due to the lack of sunlight. Temperatures below $-20°C$ are likely to favour the occurrence of ODES (Tarasick and Bottenheim, 2002; Pöhler et al., 2010), however, ODEs were also observed at $-6°C$ (Bottenheim et al., 2009). Shallow boundary layers are also likely to be beneficial (Wagner et al., 2001; Frieß et al., 2004; Lehrer et al., 2004; Koo et al., 2012), since they increase the speed of the auto-catalytic bromine release by confining the released bromine to a smaller space. The salinity of the sea ice is also an important factor. First-year (FY) ice covered by snow, which has a larger salinity than multi-year (MY) ice, is expected to be the main source of bromine (Simpson et al., 2007b). Despite being often depleted in bromide, snow covering MY ice may still play an active role in the release of reactive bromine (Peterson et al., 2019). Br_2 emissions directly from the sea ice were not observed (e.g. Pratt et al., 2013), which is likely due to a higher pH of the sea ice due to buffering (Wren and Donaldson, 2012). The salinity of FY sea ice is larger in spring, directly after its formation. This may explain why ODEs are much less pronounced in polar fall (see Nasse et al., 2019) even though meteorological conditions are similar to these in spring time.

Snow covering land surfaces may also play an active role in the release of Br_2, as several studies suggest (Simpson et al., 2005; Peterson et al., 2018). Custard et al. (2017) simultaneously measured Br_2, BrCl, and Cl_2 in the snowpack interstitial air and also provided estimates of Br_2 and Cl_2 emission rates. McNamara et al. (2020) measured the release of BrCl from snow surfaces and the dominant pathways of BrCl were identified in a box model simulation. Thomas et al. (2011) extended the 1D model MISTRA with a snow pack module and validated their results with observations at Summit, Greenland. Wang and Pratt (2017) attributed approximately 20% of the total Br_2 production to the mechanism of snow Br_2 production. Wang et al. (2019) measured atomic bromine and related it to BrO and snow-released Br_2, finding three to ten times higher levels of atomic bromine than previous estimates suggested.

From the outline above it is clear that ODEs are a complex function of chemistry and meteorology, therefore 3D simulations are useful to learn about the interaction of meteorology and chemistry in generating ODEs. Earlier studies estimated boundary layer BrO from measurements of satellite BrO vertical column densities (VCDs) (e.g. Wagner and Platt, 1998; Zhao et al., 2008) by estimating the BrO release from sea-salt aerosols produced from abraded frost flowers (Kaleschke et al., 2004; Zhao et al., 2008) or from blowing snow events (Yang et al., 2008, 2010). Toyota et al. (2011) reproduced major features of satellite BrO VCDs and in-situ measurements using a simple parameterization of bromine emissions from bulk ice and snow with the 3D air quality model GEM-AQ. Falk and Sinnhuber (2018) integrated this mechanism into the EMAC model, investigating and reproducing important features of ODEs for a full annual cycle.

In the present study, the regional 3D online numerical weather prediction system WRF-Chem is used to investigate the ODEs during Arctic spring from February 1 through May 1, 2009 since for this period of time, extensive data from observations are available from the NOAA institute or collected as part of the Ocean-Atmosphere Sea-Ice Snowpack (OASIS) field initiative for comparison with the numerical results. The chemical reaction scheme MOZART-MOSAIC is extended by bromine and

https://doi.org/10.5194/acp-2020-952
Preprint. Discussion started: 13 November 2020

Atmospheric Chemistry and Physics Discussions

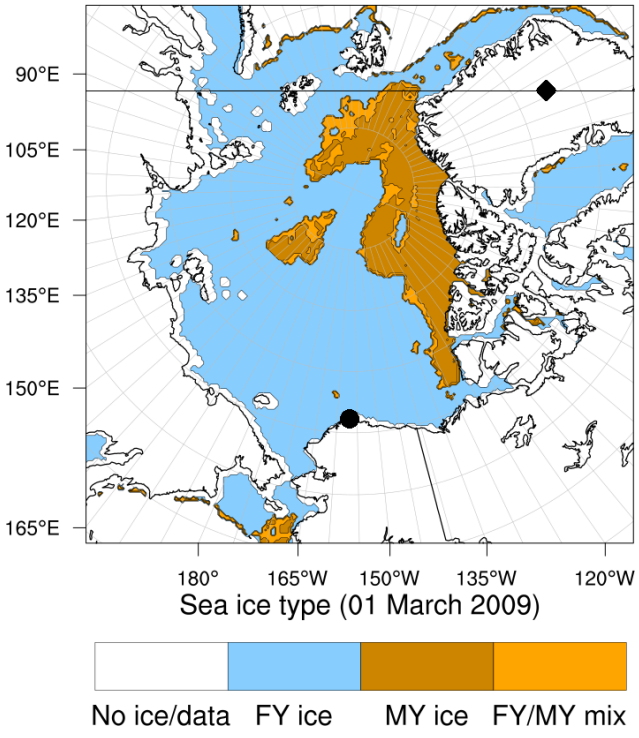

Figure 1. Domain of the simulations presented in this publication and sea ice type with the locations of (●) Utqiaġvik, Alaska, and (⧫) Summit, Greenland, respectively. The horizontal line refers to the x-coordinate in Fig. 6.

chlorine reactions to study their impact on the ODEs. The emission scheme developed by Toyota et al. (2011) is adopted and a parameter study for the reactive surface ratio (Cao et al., 2014) of the ice/snow surface is performed.

2 Model

First, the configuration of WRF-Chem (Grell et al., 2005; Skamarock et al., 2008) will be presented, then the modifications to the standard configuration will be discussed and the initial and boundary conditions will be provided.

2.1 Configuration of WRF-Chem

The physical area (displayed in Fig. 1) of 5,040 km x 4,960 km, centered north of Utqiaġvik, is modeled for the time interval of February 1, 2009 through May 1, 2009, for which GOME-2 data with a stratospheric correction for BrO VCDs (Sihler et al., 2012) as well as surface ozone and ozone sonde data are available for model evaluation.

The software Weather Research and Forecasting model coupled with Chemistry (WRF-Chem) version 3.9 is employed. WRF-Chem (Skamarock et al., 2008; Grell et al., 2005) is a state-of-the-art regional numerical weather prediction system with online computation of chemistry. Table 1 summarizes the configuration of the software. The physics modules are chosen

https://doi.org/10.5194/acp-2020-952
Preprint. Discussion started: 13 November 2020


Atmospheric Chemistry and Physics Discussions

following recommendations of the Polar WRF community (Bromwich et al., 2009; Wilson et al., 2011; Bromwich et al., 2013), the modules include the meteorology and the emission, transport, mixing, chemical reactions of trace gases as well as aerosols.

The simulation domain is centered north of Utqiaġvik using the polar stereographic projection at a true latitude of 83° with a reference longitude of 156° W. A horizontal grid resolution of 20 km for the 5,040 km x 4,960 km domain is employed, allowing comparison to GOME-2 BrO satellite data (Sihler et al., 2012) with a resolution of approximately 40 km x 30 km. In vertical direction, 64 non-equidistant grid cells with a finer resolution near the ground are used, starting with approximately 25 m at the ground level. Half of the grid cells used in the present study are in the first 2 km of the atmosphere, allowing a detailed representation of the Arctic boundary layer. The vertical grid is provided in the supplement of this manuscript.

The meteorological time step of one minute is chosen to fulfill the Courant criterion. Chemistry is updated between every meteorology time step, and radiative transfer is updated every tenth meteorological time step.

In the present model, the Mellor-Yamada-Janjic (MYJ) PBL scheme (Mellor and Yamada, 1982; Janjić, 1990) is employed, which is a 1.5-order local turbulence closure model. Prognostically determined turbulent kinetic energy is used to determine the eddy diffusion coefficients. The MYJ PBL scheme is best suited for stable to slightly unstable conditions (Mellor and Yamada, 1982).

2.2 Gas-phase chemistry

WRF-Chem offers several implementations of chemical reaction schemes. In the present study, the MOZART-MOSAIC mechanism based on MOZART-4 (Model for Ozone and Related chemical Tracers) gas-phase chemistry (Emmons et al., 2010a) is used which includes 85 gas-phase species, 237 gas-phase reactions, 49 photolysis reactions. Additional 18 gas-phase species, 73 gas-phase reactions, and 13 photolysis reactions (Herrmann et al., 2019) account for the bromine and chlorine chemistry (termed "full chemistry", see Tab. 2). Iodine is neglected since observations of reactive iodine in the Arctic region (Zielcke, 2015; Raso et al., 2017) suggest only low mixing ratios of iodine. The photolysis rates are calculated with the "Updated TUV" scheme (Madronich et al., 2002), which already contains the halogen photolysis reaction rates. The added bromine and chlorine chemical reactions are provided in the supplement.

2.3 Aerosol-phase chemistry

The MOZART-MOSAIC mechanism employs four-bin MOSAIC aerosols (Zaveri et al., 2008). In WRF-Chem, MOSAIC is implemented using a sectional approach, where size bins are defined by the upper and lower dry particle diameters. In MOSAIC, mass and number density for each bin are considered and the processes of nucleation, coagulation, condensation, evaporation, and aerosol chemistry are modeled. The mass transfer rate $k_{i,m}$ for gas species i and aerosol size section m is calculated using the parameterization (Wexler and Seinfeld, 1991)

$$k_{i,m} = 4\pi R_{\mathrm{p},m} D_{\mathrm{g},i} N_m f(\mathrm{Kn}_m, \gamma_i), \tag{1}$$

where $D_{\mathrm{g},i}$ is the gas diffusivity of species i, $R_{\mathrm{p},m}$ is the wet mean particle radius of size bin m, N_m the number density of size bin m, and $\mathrm{Kn}_m = \lambda / R_{\mathrm{p},m}$ is the Knudsen Number of size bin m with the free mean path λ. $f(\mathrm{Kn}_m, \gamma_i)$ is the transition

https://doi.org/10.5194/acp-2020-952
Preprint. Discussion started: 13 November 2020

Atmospheric Chemistry and Physics Discussions

Table 1. Summary of the configuration of WRF-Chem.

Parameter	Setting
Longwave radiation	LW RRTMG scheme (Iacono et al., 2008)
Shortwave radiation	SW RRTMG scheme (Iacono et al., 2008)
Microphysics	WSM 6-class graupel scheme (Hong and Lim, 2006)
Land-surface model	Noah Land-Surface Model (Niu et al., 2011)
Surface-layer model	Monin-Obukhov (Janjic Eta) Similarity scheme (Janjić, 1996)
Boundary-layer model	Mellor-Yamada-Janjic (MYJ) scheme (Mellor and Yamada, 1982)
Cumulus parameterization	Grell 3D ensemble scheme (Grell, 1993)
Initial and boundary data	ERA-Interim (Dee et al., 2011), MOZART-4 (Emmons et al., 2010a)
Sea ice data	OSI-403-c (Aaboe et al., 2017)
Sea surface temperature data	RTG_SST high resolution (Thiébaux et al., 2003)
Time step	1 min
Simulated time range	February 1, 2009 – May 1, 2009
Nudging	included, see text
Horizontal resolution	20 km
Longitude and latitude	252 × 248 horizontal grid cells
Vertical grid size	64 eta levels
Vertical size of the first cell	≈ 25 m
Pressure at top boundary	50 hPa
Chemistry mechanism	MOZART-MOSAIC (Emmons et al., 2010b)
	plus bromine and chlorine reactions (see supplement)
Aerosols	MOSAIC 4 bin aerosols (Zaveri et al., 2008)
Photolysis scheme	Updated TUV (Madronich et al., 2002)
Emissions	EDGAR-HTAP (Janssens-Maenhout et al., 2012)
Bioemissions	MEGAN (Guenther et al., 2006)

regime correction factor (Fuchs and Sutugin, 1971) and accounts for the interfacial mass transport limitation

$$f(\mathrm{Kn}_m, \gamma_i) = \frac{0.75\gamma_i\,(1+\mathrm{Kn}_m)}{\mathrm{Kn}_m\,(1+\mathrm{Kn}_m) + 0.283\,\gamma_i\,\mathrm{Kn}_m + 0.75\gamma_i}, \quad (2)$$

where γ_i is the accommodation coefficient for gas-phase species i taken from the CAABA/MECCA model (Sander et al., 2011). Aerosol forms of bromine are currently not implemented in the MOSAIC framework and are treated as gas-phase species. The transfer reactions of bromine gas-phase species X to aerosol-size bin m are assumed to produce species $\mathrm{X}_{\mathrm{aq},m}$ as

$$\mathrm{HBr} \rightarrow \mathrm{HBr}_{\mathrm{aq},m} \quad \text{(R17)}$$

$$\mathrm{HOBr} \rightarrow \mathrm{HOBr}_{\mathrm{aq},m} \quad \text{(R18)}$$

https://doi.org/10.5194/acp-2020-952
Preprint. Discussion started: 13 November 2020


Atmospheric Chemistry and Physics Discussions

$$\mathrm{BrONO_2} \rightarrow \mathrm{HOBr_{aq,}}_m + \mathrm{HNO_3}, \tag{R19}$$

which may produce gas-phase $\mathrm{Br_2}$

$$\mathrm{HOBr_{aq,}}_m + \mathrm{HBr_{aq,}}_m \rightarrow \mathrm{Br_2}. \tag{R20}$$

Reactions (R17)-(R20) may only occur if the aerosol is in a liquid state, and in addition, reaction (R20) requires the aerosol to have a pH of 6 or less. The heterogeneous reactions and parameters required to calculate the reaction rates are listed in the supplement.

2.4 Bromine emission scheme

Emissions of bromine species on ice/snow surfaces are parameterized following Toyota et al. (2011). Numerically, bromine emissions are coupled to vertical diffusion. In WRF-Chem, vertical (turbulent) diffusion for each species and horizontal grid cell is solved using a Peaceman-Rachford Alternating direction implicit method (Peaceman and Rachford, 1955). The bromine emissions are added as boundary conditions to the tridiagonal diffusion matrix. For the surface emission in reactions (R6), (R9), and (R10), the boundary flux for instance of (R6), $F_\mathrm{d}(\mathrm{Br_2}|\mathrm{HOBr})$ for $\mathrm{Br_2}$ due to HOBr is

$$F_\mathrm{d}(\mathrm{Br_2}|\mathrm{HOBr}) = \beta \rho_{d,0} v_\mathrm{d}(\mathrm{HOBr}) \left[\mathrm{HOBr}\right]_0 \tag{3}$$

where $\rho_{\mathrm{d},0}$ is the dry air density of the lowest grid cell and $\left[\mathrm{HOBr}\right]_0$ is the HOBr mixing ratio in the lowest grid cell. The species-dependent deposition velocity $v_\mathrm{d} \approx 1$ cm s^{-1} is calculated using the WRF-CHEM Wesely deposition module (Wesely, 1989) under an additional assumption of near-zero surface resistance. Thus, the turbulent transfer resistance dominates the deposition velocity, and the bromine emissions increase with larger wind speeds. $\beta \geq 1.0$ is the reactive surface ratio (Cao et al., 2014) of the ice/snow surface, accounting for non-flat surfaces such as ice/snow and frost flowers. For simplicity, β is set as a global value in this study, allowing to investigate the strength of bromine emissions in a parameter study. For the direct emission of bromine due to ozone oxidation of bromide, see reaction (R10) above, the factor α is used to control the emission probability

$$\mathrm{O_3} \longrightarrow \alpha \mathrm{Br_2} \tag{4}$$

and

$$F_d(\mathrm{Br_2}|\mathrm{O_3}) = \alpha\beta\rho_{d,0} v_\mathrm{d}(\mathrm{O_3}) \left[\mathrm{O_3}\right]_0. \tag{5}$$

The value of α is parameterized with a dependence on the solar zenith angle SZA (Toyota et al., 2011)

$$\alpha(\mathrm{SZA}) = \begin{cases} 0.1\% & \text{if SZA} > 85^\circ \\ 7.5\% & \text{otherwise} \end{cases} \tag{6}$$

https://doi.org/10.5194/acp-2020-952
Preprint. Discussion started: 13 November 2020


Atmospheric Chemistry and Physics Discussions

The deposition velocity for ozone is dominated by the surface resistance (Wesely, 1989), leading to $v_d(O_3) \approx 0.01$ cm s^{-1}. An emission mechanism relating to the bromide oxidation by the hydroxyl radical, see reaction (R11), is currently not implemented in the model. All sea ice is assumed to be snow covered for the simulated time range. On snow covering FY ice, it is assumed that the bromide content is infinite, so that unrestricted gaseous bromine emissions are possible, and emissions of Br_2 due to O_3 and N_2O_5 depositions are only active on snow covering FY ice. On snow covering MY ice, no bromide content but infinite chlorine is assumed. HOBr depositions only release Br_2 up to the combined depositions of gaseous and aerosol HBr whereas excess HOBr depositions release BrCl. On snow-covered land, neither bromide nor chloride content is assumed, so that excess HOBr depositions are lost. A list of the depositions and emissions added to the MOZART mechanism can be found in the supplement.

2.5 Initial and boundary conditions

ERA-Interim (Dee et al., 2011) is used to generate both the initial and boundary meteorological and sea ice cover data. Nudging of temperature, horizontal wind speed, humidity, and surface fields to ERA-Interim data ensures the validity of the simulation meteorology over the simulated three month period. Nudging is active for the entire duration of the simulation and is inactive inside the boundary layer. The nudging timescale is set to one hour. MOZART-4 results driven by GEOS-5 meteorological fields are used as initial and boundary data for all non-halogen species (Emmons et al., 2010a). For most halogen species, initial and boundary conditions are set to near-zero values. The initial mixing ratio of HBr and Br_2 are set to 0.3 ppt in the lowest 200 m of the atmosphere. The mixing ratio of $CHBr_3$ is fixed to 3.5 ppt (Toyota et al., 2014). The RTG_SST high-resolution dataset (Thiébaux et al., 2003) is used for the sea surface temperature (SST). In the present model, it is differentiated between FY and MY sea ice in order to estimate bromine emissions. For this purpose, the OSI-403-c sea ice type dataset (Aaboe et al., 2017) is used. The original dataset does not provide values for latitudes larger than about 88° due to a lack of satellite measurements for these latitudes. In the present study, these values are filled with first year sea ice. Figure 1 shows the simulation domain and the locations of FY and MY sea ice. Grid cells with a mixed FY/MY sea ice type are treated as multi-year sea ice in the bromine emission mechanism described above. Sea ice cover, SST, and sea ice type are updated online during the numerical simulations. EDGAR-HTAP (Janssens-Maenhout et al., 2012) and MEGAN (Guenther et al., 2006) are used as antropogenic emissions and bioemissions, respectively.

3 Retrieval of the tropospheric BrO VCD from GOME-2 observations

The tropospheric BrO vertical column density (VCD) is derived from GOME-2 observations as described in detail by Sihler et al. (2012). GOME-2 is a UV/visible/near-IR spectrometer with moderate spectral resolution aboard the MetOp-A satellite (Callies et al., 2000; Munro et al., 2006, e.g.) which was launched in 2006. MetOp-A operates in a sun-synchronous orbit with an equator crossing time of 09:30 LT. GOME-2 observes the backscattered and reflected sun light from near-nadir directions. With a swath-width of 1920 km, almost global coverage is achieved every day. Here it is important to note that in polar regions, the same location is observed several times during one day. The ground pixel size is approximately 80 km × 40 km.

https://doi.org/10.5194/acp-2020-952
Preprint. Discussion started: 13 November 2020

Atmospheric Chemistry and Physics Discussions

In the following, the most important retrieval steps to derived the tropospheric BrO VCD are briefly described. More details on the data analysis are provided by Sihler et al. (2012). The atmospheric BrO absorption is analyzed in the spectral range from 336 – 360 nm, yielding the so-called slant column density (SCD), which represents the integrated BrO concentration along the light path. Since the retrieved BrO SCD represents the total atmospheric column (including the stratosphere), the stratospheric partial BrO SCD has to be determined and subtracted from the total BrO SCD to yield the tropospheric BrO SCD. For that purpose, the simultaneously retrieved stratospheric SCDs of O_3 and NO_2 are utilized, from which the stratospheric BrO SCD can be estimated. It is important to note that neither meteorological nor chemical model data is applied for this retrieval step except the ECMWF potential vorticity to filter possible interferences from the stratospheric polar vortex (Sihler et al., 2012). In the final step of the analysis, the retrieved tropospheric BrO SCD is converted into the tropospheric BrO VCD. This conversion step is only based on measured quantities, particularly on the simultaneously measured O_4 SCD at 360 nm and the reflectance at 372 nm. Finally, the retrieved BrO VCDs are filtered and only measurements above a chosen sensitivity threshold of 0.5 are used.

4 Results and discussion

In the following, the results of the six different simulations described in Tab. 2 are discussed and compared to three different observational data sets:

- ground-based in-situ ozone measurements at Utqiaġvik, Alaska, and Summit, Greenland (McClure-Begley et al., 2014).
- vertical profiles of the ozone mixing ratio derived from ozone-sonde measurements in Utqiaġvik (Oltmans et al., 2012).
- maps of vertical BrO column densities from GOME-2 satellite measurements (Sihler et al., 2012).

For comparison of the observations and the simulations, three different statistical parameters are used. For model variable M and the corresponding observation variable O, the Pearson correlation R, the mean bias MB, and the root mean square error

Table 2. Parameter variation in the simulations.

condition	reactive surface ratio β	meteorological nudging	time period	chemistry
1	0.0	on	Feb. 1, 2009 – May 1, 2009	no halogen chemistry
2	1.0	on	Feb. 1, 2009 – May 1, 2009	full
3	1.5	on	Feb. 1, 2009 – May 1, 2009	full
4	2.0	on	Feb. 1, 2009 – May 1, 2009	full, $\alpha = \text{const} = 0.001$, cf. Eq. (6)
5	1.5	on	March 16, 2009 – May 1, 2009	full
6	1.5	off	Feb. 1, 2009 – May 1, 2009	full

https://doi.org/10.5194/acp-2020-952
Preprint. Discussion started: 13 November 2020

Atmospheric Chemistry and Physics Discussions

RMSE are calculated by

$$\mathrm{R} = \frac{\langle (M - \langle M \rangle)(O - \langle O \rangle) \rangle}{\sigma_M \sigma_O} \quad (7)$$

$$\mathrm{MB} = \langle M - O \rangle \quad (8)$$

$$\mathrm{RMSE} = \sqrt{\left\langle (M - O)^2 \right\rangle}, \quad (9)$$

where $\langle\ \rangle$ is the mean and σ_M and σ_O denote the standard deviations of M and O, respectively.

4.1 Surface ozone and meteorology at Utqiaġvik and at Summit

The NOAA and ESRL Global Monitoring Division Surface Ozone (McClure-Begley et al., 2014) measurements near Utqiaġvik and Summit are compared to the simulation results for the numerical grid cell closest to the observation site under consideration where the numerical results in the lowest grid cell are used. The temperature at 2 m, wind speed, and wind directions at 10 m of the Barrow Atmospheric Baseline Observatory (Mefford et al., 1994) are compared to the corresponding simulated surface fields.

Figure 2 shows simulated and observed temperatures, T in 2 m height and wind speeds u in 10 m height at Utqiaġvik. Simulations 1-5 share the meteorology shown in the left of Fig. 2 whereas results of simulation 6 with deactivated meteorological nudging are shown in the right of Fig. 2. The first eleven days in February are very cold, reaching temperatures as low as -40°C and the wind speed is very low during this period of time, which is likely to inhibit BrO emission due to the wind dependence of the emission. Both the wind speed and the temperature increase during the following three weeks, wind speeds increase to values up to 16 m s^{-1} and temperature reaches up to -5°C. On February 21, 23, and March 1, wind speed is notably under-predicted by the model with nudging. Both temperature and wind speed vary strongly during that time. From mid March onwards, temperature increases gradually with fewer day to day variations compared to the previous weeks. Simulations 1-5 predict both temperature and wind speed very well during this time period with the exception of under-predictions

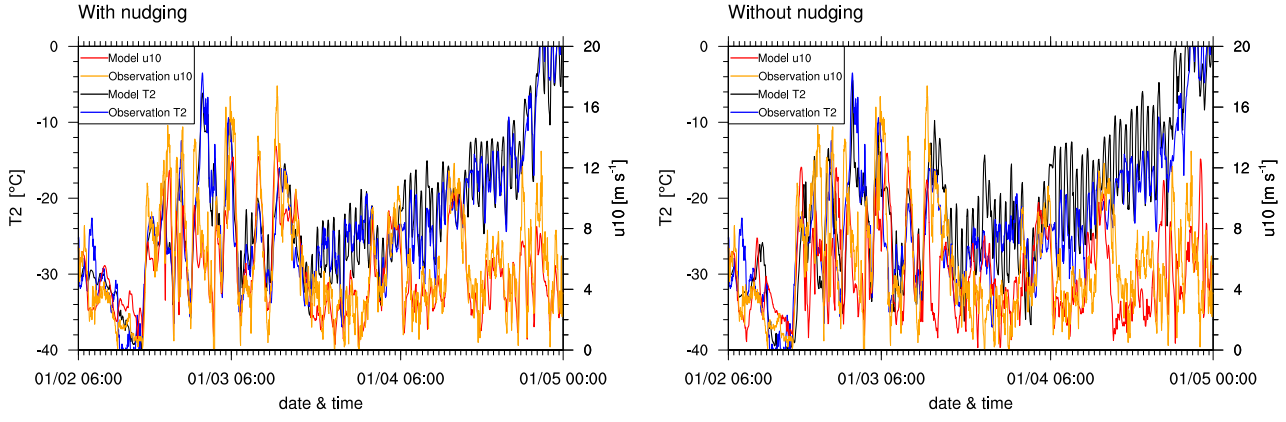

Figure 2. 2 m temperature and 10 m wind speed at Utqiaġvik in February through May 2009. Measurements are taken from the Barrow Atmospheric Baseline Observatory (Mefford et al., 1994).

https://doi.org/10.5194/acp-2020-952
Preprint. Discussion started: 13 November 2020

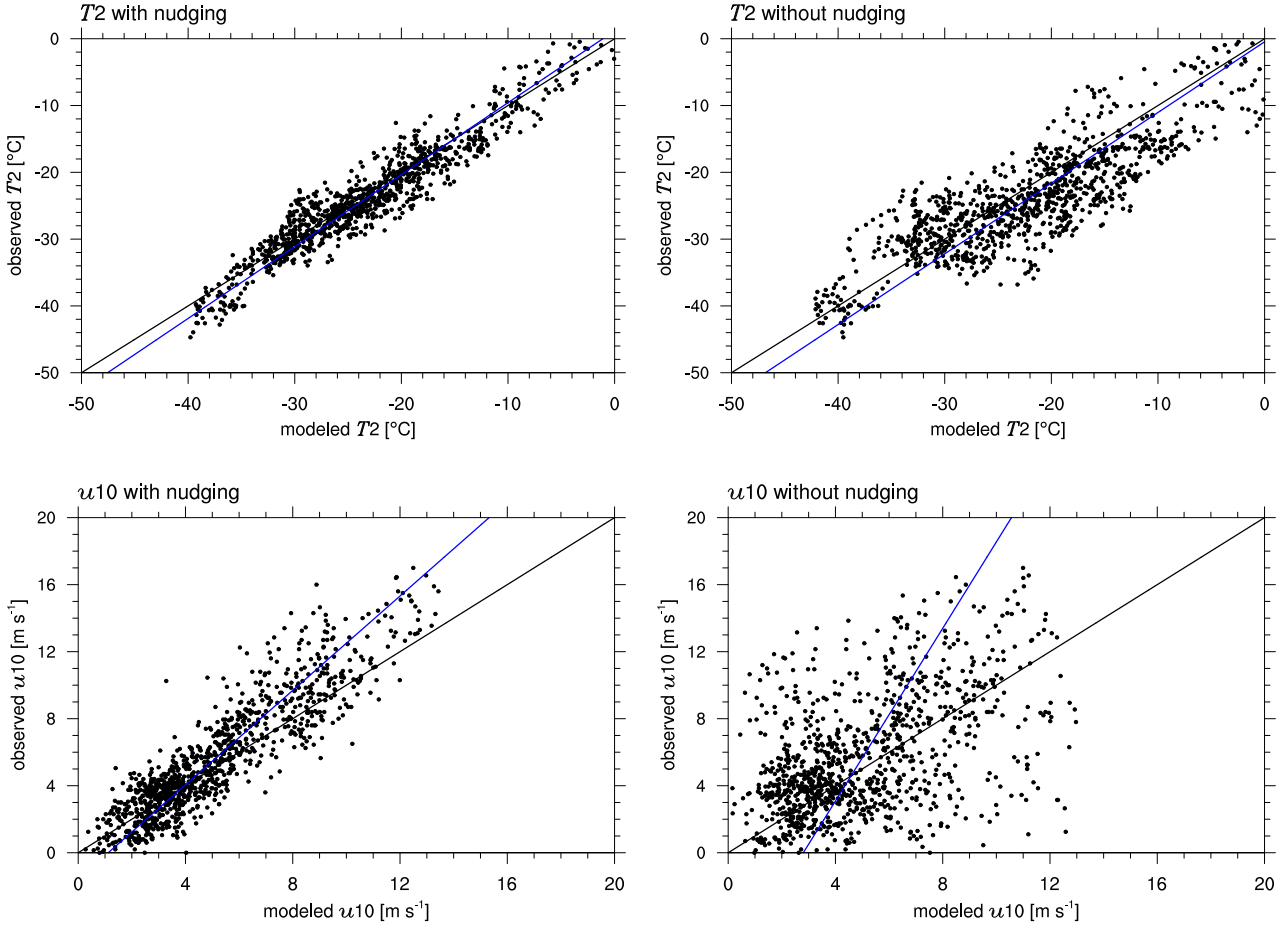

Figure 3. Correlation of observed and modeled temperature and wind speed at Utqiaġvik for the complete time range from February 1, 2009 through May 1, 2009. The black and blue lines show perfect agreement and the regression line of the simulation and the observation, respectively.

of wind speed occurring on March 16-17 and in the end of April. Simulation 6 produces higher errors in the second half of the simulation where temperature is consistently too large by several degrees in April and over-predictions of wind speed on March 18-22, April 22 and April 29. The results of simulation 6 appear not to be very realistic.

Figure 3 shows the correlation of the observed (vertical axis) and the modeled (horizontal axis) temperatures, where a correlation of unity applies if the data lie on the diagonal marked in the figure. Shown in blue is the regression line, for which the observed and measured variables are assumed to be the independent and dependent variables, respectively. The results of the entire simulation period are displayed, where the first week should be considered as spin-up time. For simulations 1-5, there is an overestimation of the temperature when it is cold, which is likely due to the lowest temperatures occurring during the spin-up time. Simulations 1-5 perform well throughout the simulation in contrast to simulation 6 with no nudging. In simulations 1-5,

https://doi.org/10.5194/acp-2020-952
Preprint. Discussion started: 13 November 2020

Atmospheric Chemistry and Physics Discussions

Table 3. Meteorology statistics at Utqiaġvik.

variable	condition	R	average of the simulated variable	MB	RMSE
2m temperature	1-5	0.962	-22.7°C	0.547°C	2.51°C
2m temperature	6	0.874	-21.5°C	1.71°C	5.05°C
10m wind speed	1-5	0.903	5.13 m s^{-1}	-0.518 m s^{-1}	1.64 m s^{-1}
10m wind speed	6	0.492	4.99 m s^{-1}	-0.655 m s^{-1}	3.28 m s^{-1}
10m wind direction	1-5	0.801	131°	3.76°	55.4°
10m wind direction	6	0.423	157°	29.51°	100.8°

a maximum deviation in temperature of about 8°C occurs and in simulation 6, a stronger temperature difference of up to 20°C is observed.

The statistical parameters, cf. Eq. (9), at Utqiaġvik for the entire time range are shown in Table 3. The simulations with nudging perform better in all regards, emphasizing the necessity of data assimilation. Temperature is predicted best with almost perfect correlation and relatively small mean bias and RMSE. Temperature is over-predicted in all simulations by approximately 0.55°C and 1.71°C for simulations 1-5 and 6, respectively. Colder temperatures are generally favorable for ODEs, both by changing the boundary layer configuration and affecting chemical reaction constants, which could result in an underestimation of ODEs. Both wind speed and direction are predicted less accurately, which might result in wrong source locations or times of the occurrence of ODEs; this is likely to explain some of the differences between simulations and observations. Wind speed is underestimated on average by about 0.52 m s^{-1} and 0.66 m s^{-1} for simulations 1-5 and 6, respectively, which may contribute to a slight underestimation of BrO emission due to the dependence of the deposition velocity on wind speed.

Figure 4 shows modeled and observed surface ozone and BrO at Utqiaġvik and at Summit. Only results of simulations 1 and 3 are shown for visual clarity. Figure S1 of the supplement displays ozone mixing ratios modeled by simulations 1-4 and 6. The correlations of modeled and observed ozone can be seen in Figure 5. Statistics are summarized in Table 4. Simulation 2-5 perform considerably better than simulation 1 for which halogen chemistry is turned off. Simulation 3 with enhanced emission performs best with the correlation increasing from -0.31 to 0.644 compared to simulation 1. Quite a few ODEs are not captured by simulation 4. This suggests a strong underestimation of BrO emission without a direct emission of BrO due to ozone. A possible conclusion is that the bromine explosion mechanism is insufficient to explain ODEs in the Arctic, or the present bromine explosion scheme is incomplete for instance with respect to emissions of bromide containing aerosols due to blowing snow and/or regions of increased β such as frost flowers. On March 4 a ODE is predicted by simulation 4 which, however, is not seen in the observations. The model predicts too large wind speeds for the preceding days, causing larger BrO emissions that ultimately result in a predicted ODE being advected to Utqiaġvik. For the first three weeks of February, the observations and results of simulations 2-6 are similar to these of simulation 1 in which halogen reactions are turned off, but afterwards, they differ increasingly. This suggests a weak initial influence of halogen chemistry during the first three weeks of February which might be due to the low wind speeds during this time or due to the weak solar irradiation. Partial ODEs occur on February 14, 17, 19, and 22, 2009. The first full ODE in the observations occurred on the February 13, which is predicted by the model only

https://doi.org/10.5194/acp-2020-952
Preprint. Discussion started: 13 November 2020

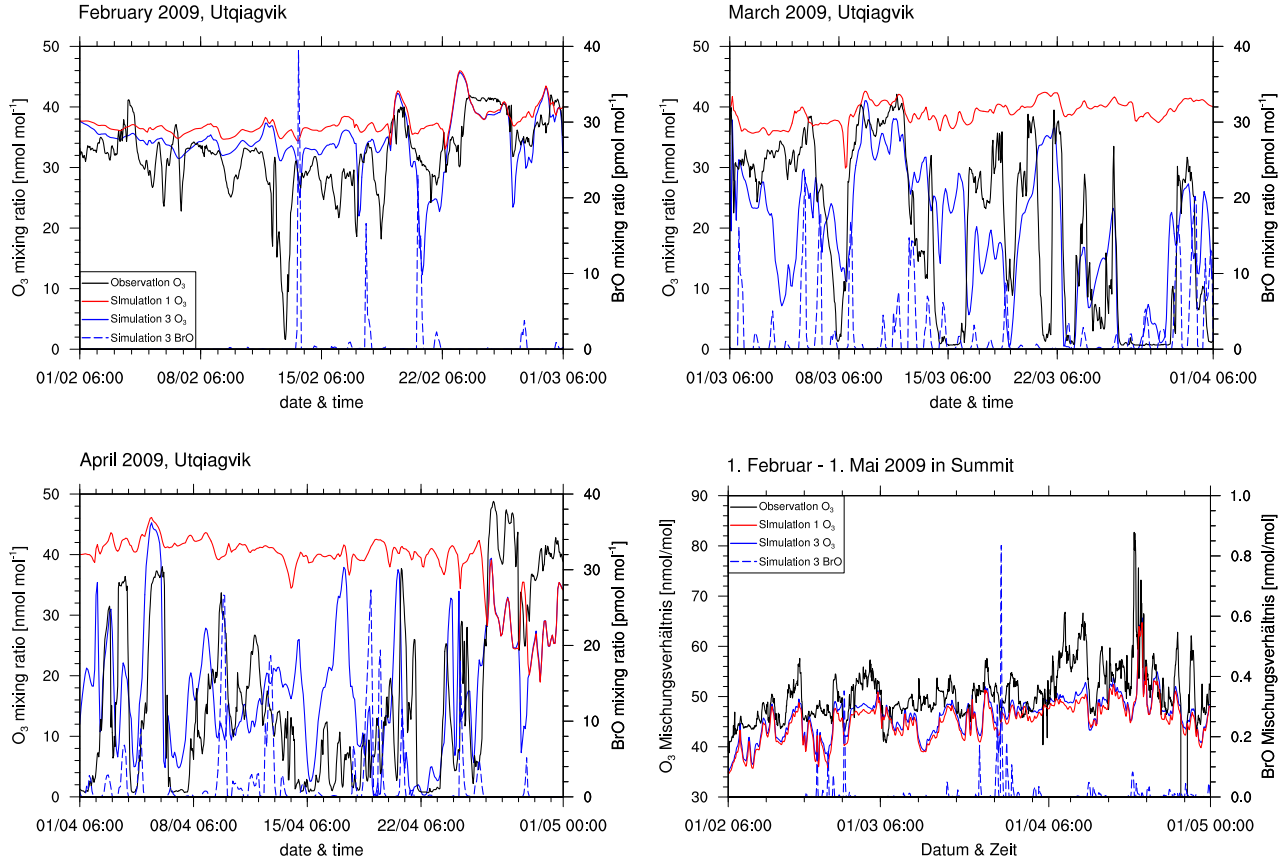

Figure 4. Ozone and BrO mixing ratios at Utqiaġvik and at Summit from observations and simulations 1 (no halogens) and 3 (increased emissions, $\beta = 1.5$). The figures share the legend.

as a partial ODE with one day of delay. The partial ODE observed on February 17 is found in simulations 2-5 with a delay of a few hours; simulations 3 and 4 find a stronger ozone depletion more consistent with the observations. On February 21, 2009, simulations 2-3 and simulations 4-5 predict partial and full ODEs, respectively, which are not seen in the observations. The strength of the ODEs in February is underestimated by the model. A possible cause for this is an overestimation of halogen deposition over land, which can be seen in the comparison to satellite data and is discussed in section 4.3. Most of the model BrO capable of reaching Utqiaġvik can only be produced at Bering Sea during February due to a lack of sunlight in the northern regions. Since BrO over land is removed too quickly in the model, only trajectories that go mostly over the sea ice are able to transport BrO from Bering Sea to Utqiaġvik.

In March, both simulations and observations agree in the occurrence of at least partial ODEs during most of the month whereas times without any ozone depletion at all are rare. Around March 4, the model predicts a partial ODE in simulations 2-4, whereas simulation 6 predicts a full ODE, neither of which is found in the observations. Four days later, all simulations predict a partial ODE even though a full ODE is seen in the observations. The following ODE-free time period until March 13

https://doi.org/10.5194/acp-2020-952
Preprint. Discussion started: 13 November 2020

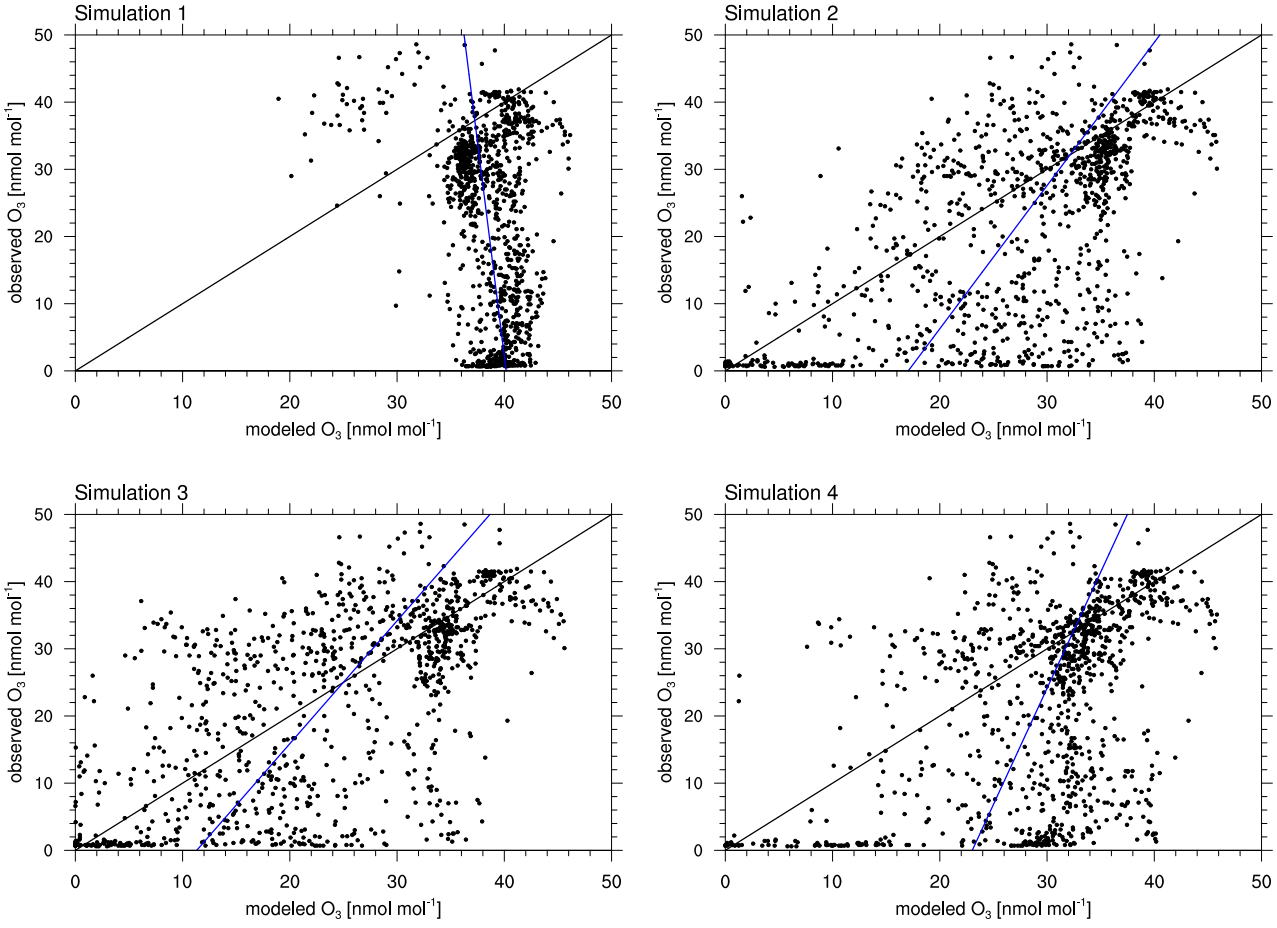

Figure 5. Correlation of observed and modeled ozone at Utqiaġvik for the complete time range of February 1, 2009 through May 1, 2009. The black and blue lines show perfect agreement and the regression line of simulation and observation, respectively.

is predicted in agreement with the observations, however, the full ODE on March 15 appears as partial ODE in all simulations, and the simulations with enhanced emission find the partial ODE to continue for three more days. The ODE on March 19 is found in simulations 2-6. The simulations predict a near-full recovery of ozone levels over three days, which, however, is interrupted in the observations on March 21. The following ODE episodes are captured quite well by the simulations with an over-prediction of ozone levels on March 25 and March 28. ODEs around April 1, 14, and 18 are underestimated in the simulations, whereas all other ODEs and ozone regeneration episodes are predicted quite well. At the end of April, the observations find enhanced ozone levels which are not captured by the model, not even by the simulations without the halogens. The enhanced ozone levels in the observations might be due to Arctic haze, i.e. enhanced photochemical ozone formation due to air pollution originating from lower latitudes. The domain modeled in this work (see Fig. 1) does not consider the lower latitudes, so that the simulation itself cannot predict the production and transport of Arctic haze. However, pollution from the

https://doi.org/10.5194/acp-2020-952
Preprint. Discussion started: 13 November 2020

Atmospheric Chemistry and Physics Discussions

Table 4. Statistics at Utqiaġvik and Summit for the ozone mixing ratio for February 1, 2009 through May 1, 2009.

Simulation	location	R [-]	average of the simulated variable [nmol/mol]	MB [nmol/mol]	RMSE [nmol/mol]
1	Utqiaġvik	-0.310	38.3	15.80	21.9
2	Utqiaġvik	0.617	27.6	5.09	12.1
3	Utqiaġvik	0.644	23.7	1.08	10.9
4	Utqiaġvik	0.454	29.5	6.97	14.3
6	Utqiaġvik	0.430	24.0	1.41	14.1
2	Summit	0.689	46.3	-4.31	5.80

lower latitudes might be correctly modeled by the MOZART-4 model and thus be present in the lateral boundary conditions. The model does not find these enhanced ozone levels, which suggests inaccuracies in the MOZART-4 boundary conditions. Simulation 3 finds a partial ODE on April 29, which is not present in the observations. The other simulations also find a slight decrease in the ozone mixing ratio, however, for these simulations, the BrO levels are not predicted to be large enough for an ODE to happen. Summarizing the entire period of three months, simulation 1 shows two ODEs where none were observed. Twenty-two ODEs are identified in the observations, half of which are found by simulation 2. Simulation 3, however, identifies four additional ODEs compared to simulation 2 which were not found in the observations. Simulation 3 misses only six of the 22 observed ODEs.

The results of simulation 6 differ strongly from the other simulation results starting mid March and the correlation coefficient R of 0.435 compared to simulation 2 with R = 0.62. The RMSE is 14.1 nmol/mol compared to 12.1 nmol/mol. The mean bias is improved, but this is simply due to the enhanced emissions, resulting in more ODEs and not due to actually predicting the ODEs better. All statistics are worse compared to simulation 3. As discussed previously in this section, simulation 6 predicts meteorology much worse due to the lack of nudging, which also leads to wrong predictions in the ozone mixing ratio. As can be seen in the correlation plots, simulations 2 and 4 rarely find ODEs were there are none in the observations. There is a notable accumulation of points in all 4 simulations at ozone mixing ratios of about 30–40 nmol mol^{-1} for both the observations and the model. In this range of ozone mixing ratios, both the model and observations do not show any ODEs. Halogen chemistry, which has large uncertainties regarding the chemical reactions and the source of bromine, is less important in this case, which explains the high density of points in this regime. This accumulation is denser for simulations with weaker bromine emissions, since those simulations predict ODEs less often which do not exist in the observations. There is an additional accumulation of points around an ozone mixing ratio of zero in both model and observations for simulations 2-4, which are ODEs found by both model and simulation. This accumulation is less dense for simulation 4 compared to simulations 2 and 3. Simulation 4 performed worst regarding both mean bias and RMSE. In simulation 4, there is an accumulation of points at around modeled ozone values of 30 nmol mol^{-1} and observed ozone values of zero, which are the missed ODEs by the simulation which suggests an underestimation of the occurrences of ODEs. Simulation 4 with a strongly enhanced $\beta = 2.0$ but a reduced BrO emission due to direct bromide oxidation by ozone during daytime ($\Phi = 0.1$) suggests that the bromine explosion mechanism alone is insufficient to properly predict the bromine production.

https://doi.org/10.5194/acp-2020-952
Preprint. Discussion started: 13 November 2020

Atmospheric Chemistry and Physics Discussions

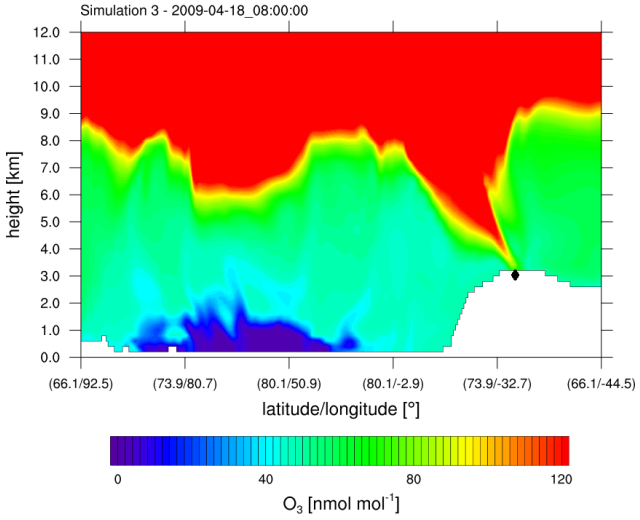

Figure 6. Ozone mixing ratio obtained from simulation 3 (β = 1.5) against height along a horizontal line through Summit, cf. Fig. 1. A tropopause fold reaches Summit (⧫).

Simulations 2-4 and 6 reproduce ozone levels and ODEs much better than simulation 1, where the mean bias is smaller by at least 9 nmol/mol. For simulation 3, all statistics are improved compared to the base simulation 2, with both the correlation and RMSE being only slightly better and the mean bias being about 80% smaller (1.1 nmol mol^{-1} vs. 5.1 nmol mol^{-1}) than in simulation 2. Figure 5 shows a strong increase in the number of ODEs that occur in the model but not in the observations, which explains the strongly improved mean bias while the other statistics only improved slightly.

At Summit, ODEs were found by none of the simulations and not in the observations which lack data for April 29 as can be seen in Fig. 5. The differences between a simulation without halogens and with halogens are negligible. Ozone mixing ratios are under-predicted with a mean bias of -4.3 nmol/mol for simulation 2. This is in contrast to Utqiaġvik, where ozone was generally over-predicted. In April, ozone levels at Summit are found to exceed 60 nmol mol^{-1} for several time periods in the observations. This is probably due to the high elevation of 3,200 m above sea level of Summit in contrast to Utqiaġvik. At Summit, the time period with the highest ozone level is also found by the model which is due to stratospheric ozone, reaching the troposphere due to a tropopause fold event as shown in Fig. 6. The other time periods of enhanced ozone levels found by the observations may also be due a tropopause fold or possibly Arctic haze events.

4.2 Vertical ozone and temperature profile at Utqiaġvik

Ozone sonde sounding data (Oltmans et al., 2012) produced near Utqiaġvik are used to validate vertical ozone profiles. Measured ozone and potential temperature for the upward flight of the sonde in the first 2 km are shown in Figs. 7 and 8 together with the simulation result of the column of the nearest grid cell. The simulation result is interpolated linearly in time to the starting time of the sonde flight.

https://doi.org/10.5194/acp-2020-952
Preprint. Discussion started: 13 November 2020

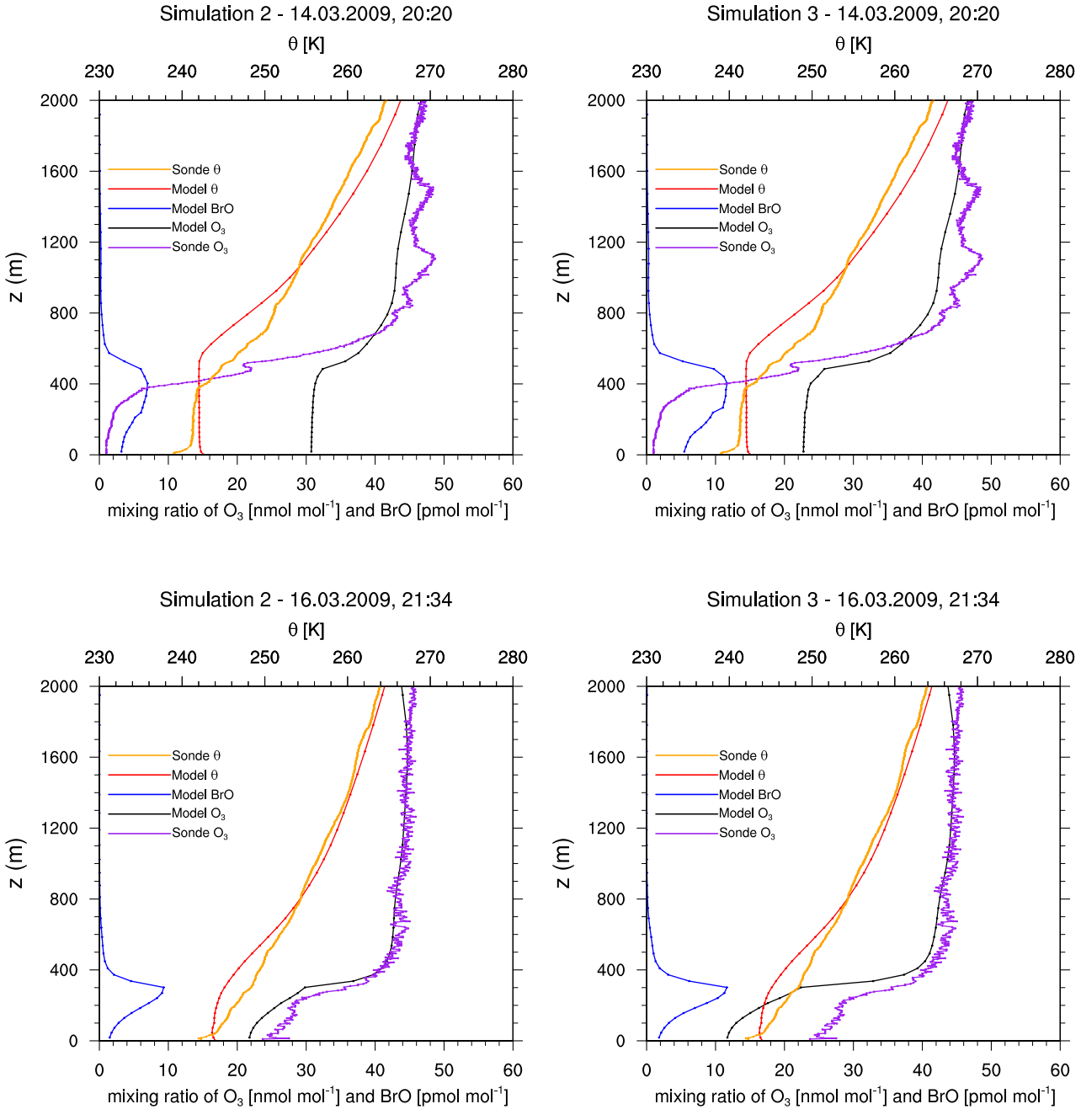

Figure 7. Vertical profiles of measured and modeled ozone, of potential temperature θ, and of BrO at Utqiaġvik on March 14 (top) and 16 (bottom), 2009. Measurements are from upward flights using ozone sondes (Oltmans et al., 2012).

Figures 7 and 8 show vertical profiles at Utqiaġvik for various dates. For March 14, the model fails to find the shallow surface inversion (boundary layer height smaller than 50 m) possibly due to a lack of vertical resolution. The boundary layer height of

https://doi.org/10.5194/acp-2020-952
Preprint. Discussion started: 13 November 2020

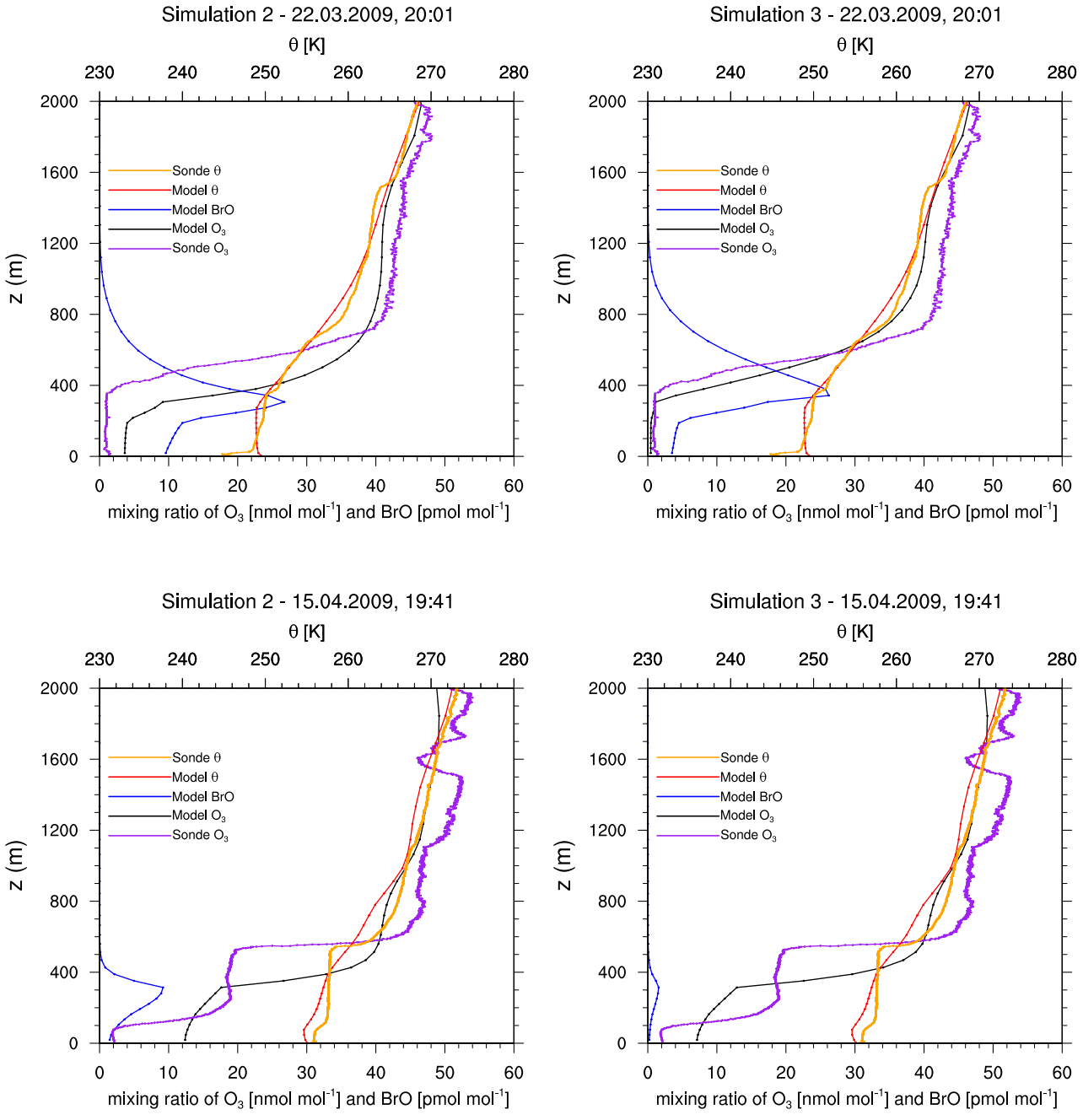

Figure 8. Vertical profiles of measured and modeled ozone, of potential temperature θ, and of BrO at Utqiaġvik on March 22 (top) and April 15 (bottom), 2009. Measurements are from upward flights using ozone sondes (Oltmans et al., 2012).

https://doi.org/10.5194/acp-2020-952
Preprint. Discussion started: 13 November 2020


Atmospheric Chemistry and Physics Discussions

about 350 m in the observation is over-predicted by approximately 200 m by the model, which might also partially explain the finding of a partial ODE by the model instead of a full ODE as seen in the observations. For this day, simulation 3 performs slightly better than simulation 2. Two days later, both the observations and the simulations show partial ODEs. Simulation 2 predicts the ozone profile very well. The temperature profiles are quite different, however, both model and observations show an inversion at a similar, low height. For March 22, the enhanced emission case correctly predicts a full ODE, capturing both ozone and temperature profile quite well. The model is however unable to capture a surface inversion. On April 15, a surface inversion with a second inversion at approximately 500 m is found in the observations. The MYJ PBL scheme also predicts a surface inversion, however it fails to predict the second inversion properly, as can be seen by the lack of a second ozone plateau. While the model is unable to capture the complex boundary layers perfectly, the ozone profiles shows many similarities to the observed profile. For a better prediction, more grid levels closer to the surface and improvements to the PBL schemes might be needed. Even that, however, might not be sufficient, since PBLs in the Arctic can be influenced by very small-scale structures such as open leads, which would require high-resolution sea ice data. Additionally, an accurate modeling of surface inversions might require very high vertical resolutions which are difficult to obtain in a synoptic scale simulation.

4.3 Tropospheric BrO VCDs

GOME-2 satellite tropospheric BrO VCDs (Sihler et al., 2012) described in section 3 are compared with BrO VCDs evaluated from the numerical simulations. All satellite BrO orbits of the same day are averaged and plotted into one figure, where missing satellite data are neglected. Since stratospheric BrO is not generated in the present model, all BrO predicted by the model is of tropospheric origin. Thus, model BrO VCDs are calculated by integrating BrO concentrations vertically from the bottom to the top of the calculation domain. Simulation results are stored every two hours starting at 00:00 UTC. Each output is assigned a 60° cone centered on a longitude, conforming to GOME-2 orbits for that time. The BrO VCDs are averaged with their neighboring cones with a weight of unity at the cone center, and decreasing linearly to zero at the edge of the cone. This procedure is a linear time interpolation and smoothes the resulting model BrO VCDs. Figure 9 displays the simulated instantaneous BrO VCDs on March 8, 2009 16:00 UTC and 18:00 UTCO. On the left there are two of the twelve full BrO

https://doi.org/10.5194/acp-2020-952
Preprint. Discussion started: 13 November 2020

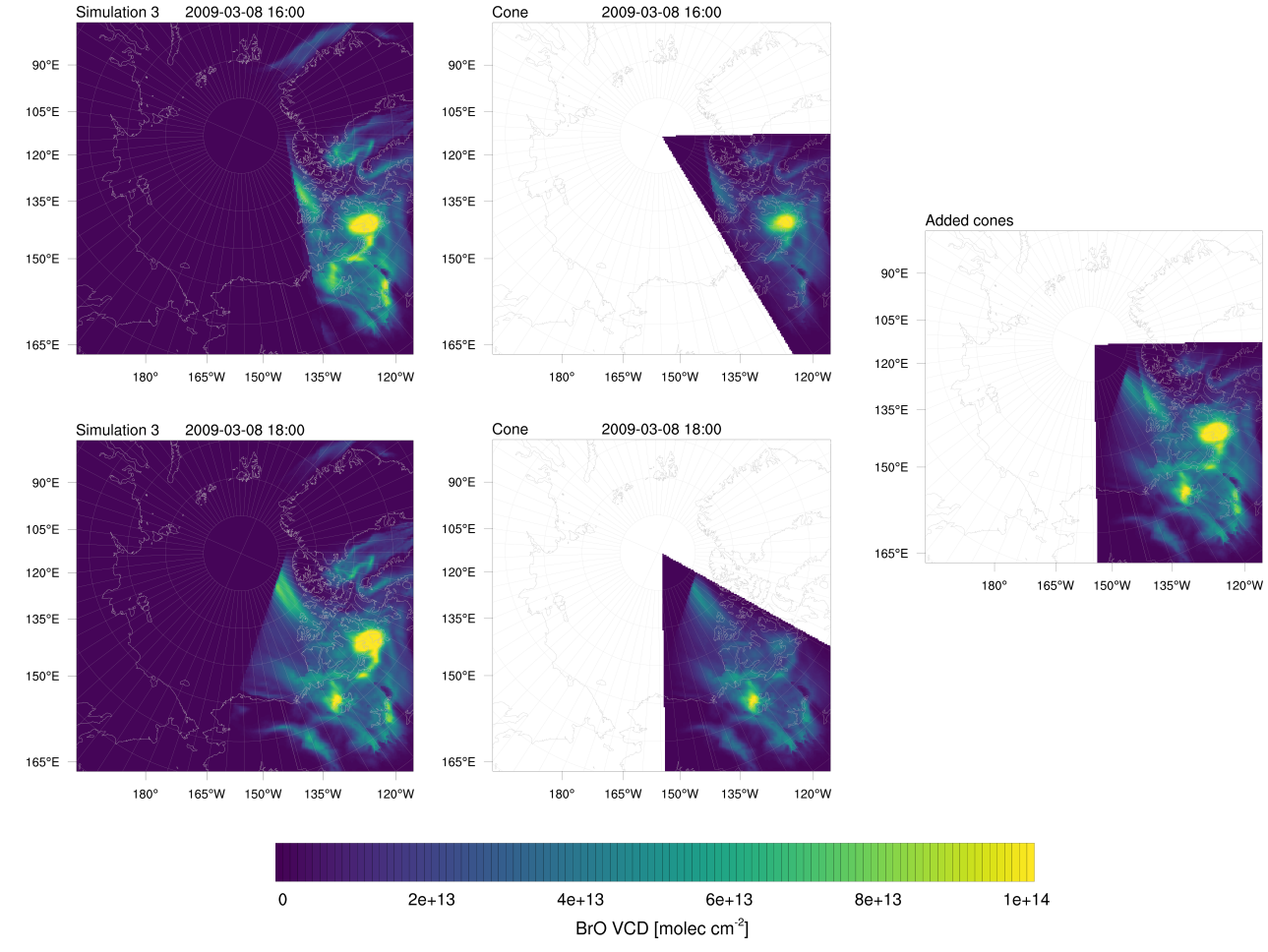

Figure 9. Illustration of the averaging of modeled BrO VCDs. Shown is March 8, 2009 16:00 and 18:00 UTC. Left: Full instantaneous BrO VCDs. Center: Corresponding 60° cone. Right: Added cones.

https://doi.org/10.5194/acp-2020-952
Preprint. Discussion started: 13 November 2020

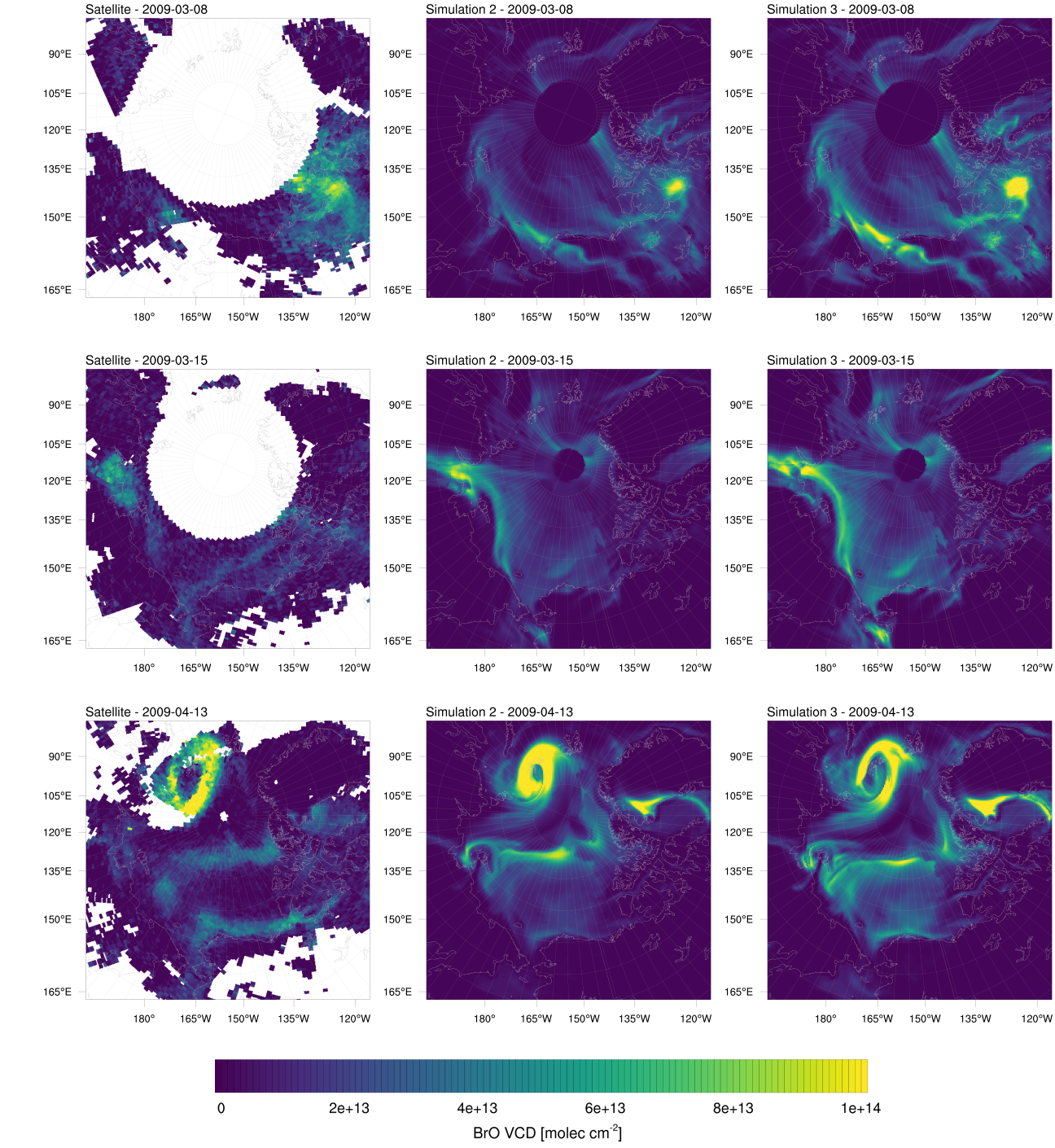

Figure 10. BrO VCDs on selected days in the year 2009. Left: Satellite measurements. Center: Simulation 2 ($\beta = 1.0$). Right: Simulation 3 ($\beta = 1.5$).

https://doi.org/10.5194/acp-2020-952
Preprint. Discussion started: 13 November 2020


Atmospheric Chemistry and Physics Discussions

VCDs saved for each day, on the middle the corresponding 60° cone multiplied by a weight of unity at the center, which linearly decreases to zero at the edges of the cone. On the right, the added cones are shown. This procedure is done each day for all twelve timepoints. Thus twelve cones, not just the two cones shown in Fig. 9, are added for the average of one day, covering the whole domain.

Figure 10 shows daily averages for the satellite data and simulations 2 and 3 on selected days. On March 8, both the model simulation and the observations show a high BrO VCD in Nunavut, including King William Island. However, the models predict BrO VCDs to be strongly concentrated in a small area whereas the satellite BrO cloud is spread out more and reaches deeper into the Canadian mainland. On March 15, both model simulations and satellite observations find a bromine cloud over the Laptev Sea, reaching to the Siberian land mass. The modeled BrO VCDs are more pronounced, with simulation 3 having a different distribution of BrO being less consistent with the observations than simulation 2. The enhanced emissions in simulation 3 cause a stronger ODE in that region, which in turn depletes BrO in the ozone depleted area. Ozone mixes back into the ozone-depleted area from the edges of an ODE, which allows BrO to form there which is the reason for the elevated BrO-levels seen at the edges of the ODE. The bromine cloud is predicted by the model to extend to Chuckchi Sea in a thin stripe, which is barely seen in the observation. In both model results, a small BrO cloud in Hudson Bay is found, which is more pronounced and less consistent with the observations for simulation 3. On April 13, a ring-like BrO structure can be seen north or Kara Sea. The BrO-free center of the ring is due to an ozone depletion. Both simulations correctly find a BrO-free area near the north pole. An enlarged ODE is predicted, resulting in a thinner ring more consistent with the observations. The model, however, under-predicts BrO clouds near the Alaskan coast and finds enhanced BrO VCDs on Greenland in contrast to the observations. In summary, both simulations 2 and 3 appear to be successful in capturing the general structures. Some of the differences might be explained by a higher model resolution, 20 km × 20 km, compared to the satellite data with a resolution of 40 km × 30 km, resulting in more detailed structures in the model. Other differences might be explained by the already discussed errors in the meteorology and under-predicted of BrO over land discussed below.

Figure 11 shows monthly averages for the satellite data and results of simulations 2 and 3. The simulations under-predict BrO over land and near coasts which is most likely due to the assumptions in the emission scheme. In the model, it is assumed that snow surfaces have no salt content, which makes depositions of bromine species (excess HOBr is lost) over land a sink, opposed to depositions over MY ice being neutral (excess HOBr is released as BrCl) and over FY (HOBr always releases Br_2) being a source for bromine in most cases. With a deposition velocity of 1 cm s^{-1} and a boundary layer height of 200 m, bromine is removed at a timescale of approximately 5 hours over land by surface depositions and possibly even faster by depositions to aerosols. BrO VCDs are also under-predicted near the boundaries, which is due to the value of zero of halogens at the boundary. The model over-predicts BrO VCDs at Baffin Bay and at most locations featuring FY sea ice with the exception of Bering Sea, probably due to its proximity to a domain boundary. The over-prediction over FY sea ice is not surprising with the assumption of unlimited BrO in FY sea ice. A relaxation of this assumption, e.g. by allowing finite salt content could solve the issues both, over snow covering FY ice by limiting the bromine emissions and over land, by allowing salt content of more than zero and storage instead of loss of deposited bromine. The model prediction for BrO in February is generally too small, which is probably

https://doi.org/10.5194/acp-2020-952
Preprint. Discussion started: 13 November 2020

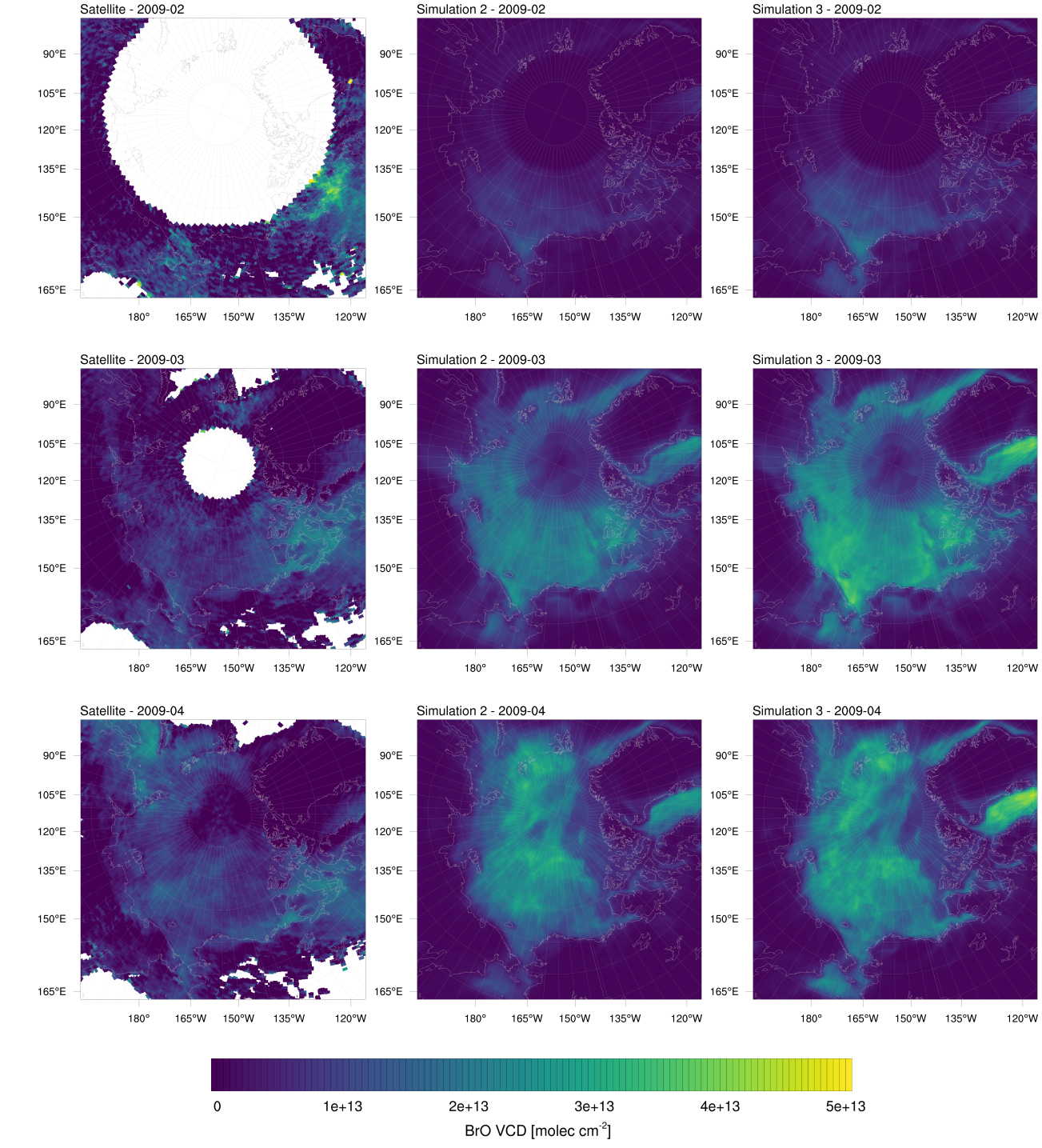

Figure 11. BrO VCDs in the year 2009 averaged over one month. Left: Satellite measurements. Center: Simulation 2 ($\beta = 1.0$). Right: Simulation 3 ($\beta = 1.5$).

https://doi.org/10.5194/acp-2020-952
Preprint. Discussion started: 13 November 2020

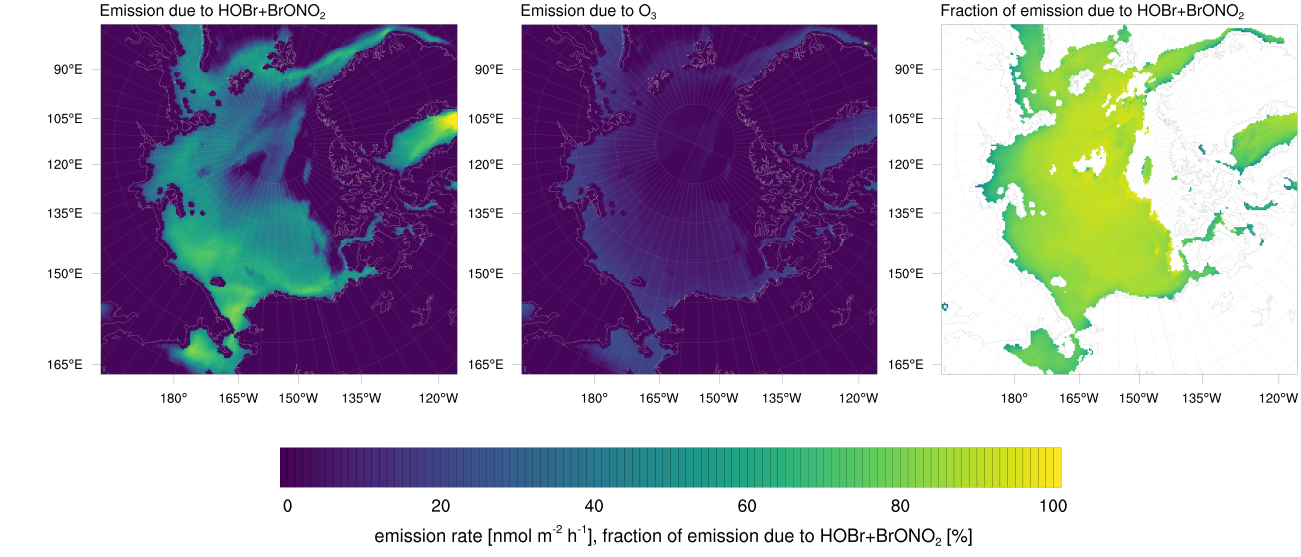

Figure 12. Emission rate of Br_2 due to HOBr+$BrONO_2$ (left) and due to bromide oxidation by ozone (center) for simulation 3, averaged over the complete simulation period. Ratio of Br_2 emissions due to HOBr and $BrONO_2$ to total Br_2 emissions on FY ice (right).

due to a lack of sunlight at higher latitudes and the under-prediction of BrO over land. It should be noted that the satellite data is quite incomplete during February and biased towards the end of February, also due to a lack of sunlight necessary for satellite measurements in early February, whereas the model VCDs weighs all of February equally.

The emission rate of Br_2 due to HOBr+$BrONO_2$ and due to bromide oxidation by ozone averaged over the entire simulation period is shown in Fig. 12 for simulation 3. In Fig. 13, the production of Br_2 is shown at coordinates 178 W, 78 N plotted against time. The location has been chosen because it is over FY sea ice and is a strong production site for the bromine that

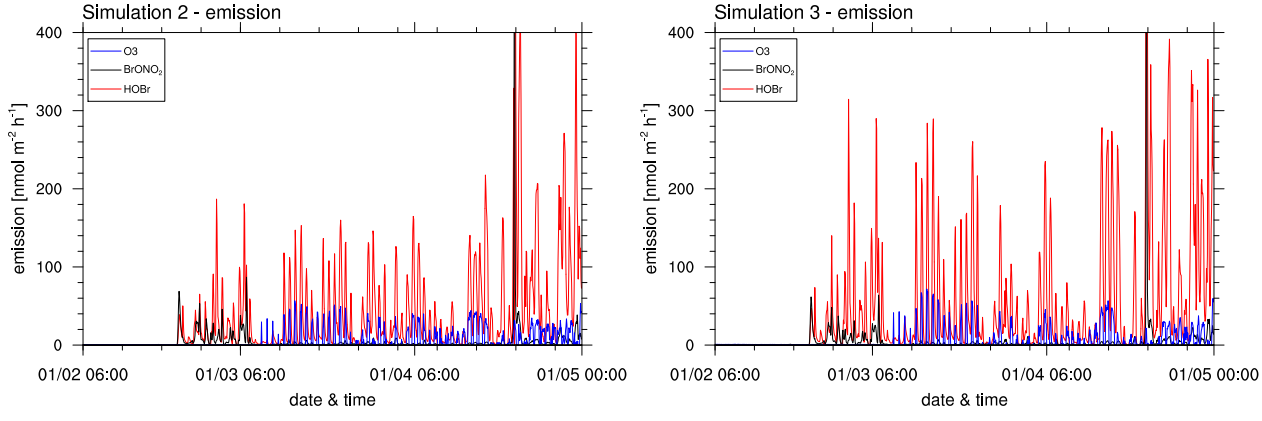

Figure 13. Emission rate of Br_2 due to HOBr, $BrONO_2$ and due to bromide oxidation by ozone at coordinates 178 W, 78 N for simulations 2 ($\beta = 1$) and 3 (β= 1.5).

https://doi.org/10.5194/acp-2020-952
Preprint. Discussion started: 13 November 2020

Atmospheric Chemistry and Physics Discussions

may affect ODEs at Utqiaġvik. As can be seen in these figures, most of the bromine is produced by HOBr, i.e. the bromine explosion mechanism, whereas the oxidation of bromide by ozone provides an initial seed of the bromine formation which then is enhanced by bromine explosion where $BrONO_2$ plays a smaller role than HOBr. Due to a lack of sunlight, bromine is produced only during the second half of February by the bromine explosion and after March 1, 2009, by the bromide oxidation due to ozone. In the present parameterization, the latter strictly requires a SZA of less than 85° for a fast release, whereas the bromine explosion mechanism has a more continuous dependence on SZA. The Br_2 photolysis needed by both emission mechanisms requires relatively long-waved light and may thus occur even at SZAs slightly above 90°. The bromine explosion additionally requires HO_2 in order to produce HOBr. HO_2 is mostly formed by a photolysis of various organic species with short-waved UV and thus occurs generally at smaller SZA, however, it can also be supplied by reactions involving organic compunds, NO_x and/or OH or by their transportation from lower latitudes. Thus, in the present parameterization, the bromine explosion may occur locally at higher SZAs than the bromide oxidation due to ozone.

For a simulation of three month, it should be expected that errors in the simulation pile up, especially considering the nonlinear stochastic nature of ODEs. The meteorological state should be consistent due to the data assimilation via nudging, however, the errors in the chemistry model could grow large over time. As an example, wrongly predicting an ODE probably causes a delay of an ODE at a later date due to the lack of O_3, reducing bromine emissions. A test for this is performing a new start of a simulation at a later date, where no ODEs occurred and in which the atmosphere is clean of bromine. For this purpose, simulation 5 was conducted, which is identical to simulation 3 except that the simulation starts on March 16 using ERA-Interim and MOZART-4 data as well as a near-zero bromine concentration, as described in section 2.5. These new simulation results are then compared to simulation 3 which started in February.

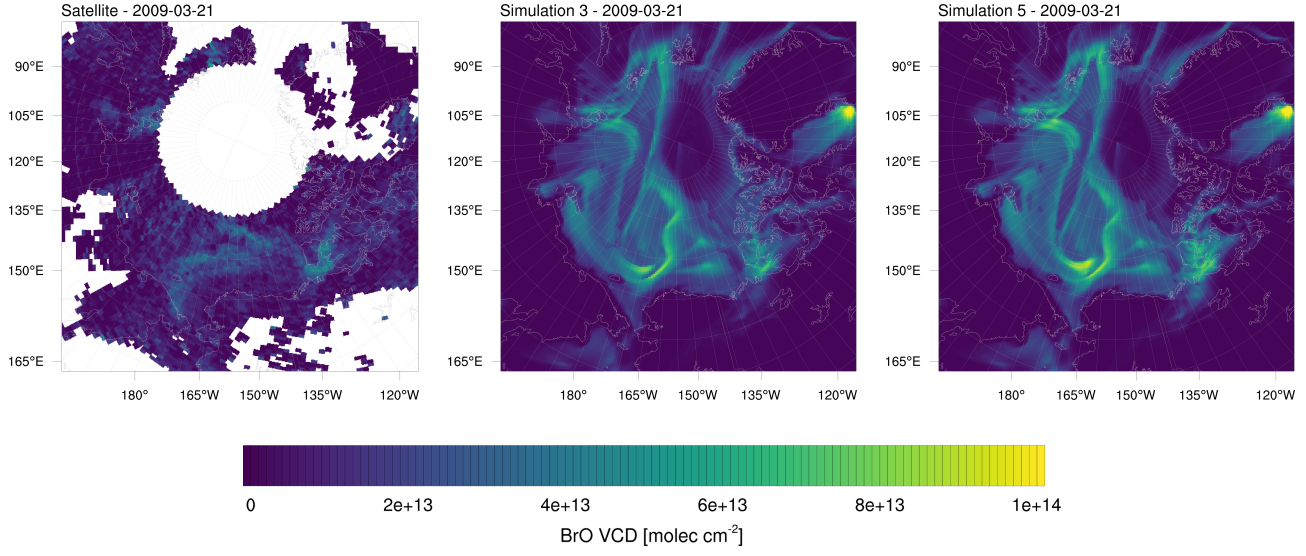

Figure 14. BrO VCDs on March 21, 2009 from observations (left) and simulations initiated on February 1 (simulation 3, center) and March 16 (simulation 5, right). The simulations differ only in the start time.

https://doi.org/10.5194/acp-2020-952
Preprint. Discussion started: 13 November 2020


Atmospheric Chemistry and Physics Discussions

It is found that these two simulations become very similar after approximately 5 days, see Fig. 14 which shows the BrO VCDs. After approximately 8 days, the BrO VCDs become nearly indistinguishable. Average BrO concentrations in April are not shown here, but are also nearly identical for both simulations.

Reasons for the two simulations with different staring times to show so similar results after a few days is due to a combination of several factors. While there is no chemical nudging, the chemical boundary conditions strongly affect the simulation and act similar to a chemical nudging. Assuming a constant wind speed of 20 km/h (corresponding to approximately 5.5 m s^{-1}), a chemical species can be transported from a 2,000 km distant boundary to the center of the domain on a time scale of as low as four days. Due to the meteorological nudging, chemical boundary conditions are transported in the same way in both simulations.

Chemistry boundary conditions transported over land or in the free troposphere behave similar in simulations 3 and 6, since several aspects of chemistry over land and in the free troposphere are nearly unaffected by the addition of halogen chemistry. Thus, chemical species coming from the lateral boundary condition will only be affected by the halogen chemistry once they reach the sea ice or are mixed into the boundary layer from aloft.

The emission of bromine due to bromide oxidation by O_3 is independent of reactive bromine mixing ratios and not of auto-catalytic nature as in the bromine explosion mechanism. While it is only responsible for small fraction of emitted bromine, it produces the initial bromine needed for a bromine explosion. The present emission scheme can be very fast, producing full ODEs in less than a day. All of these effects allow ozone coming from the lateral boundary condition to be depleted in a similar way in simulations 3 and 6 even with leftover bromine from a previous ODE.

5 Conclusions

Three-dimensional unsteady simulations of ozone depletion events in the Arctic from February 1, 2009 through May 1, 2009 have been performed using WRF-Chem. Simulations with different parameter settings are compared to observations from different sources at Utqiaġvik, Alaska and Summit, Greenland. A simulation using standard MOZART-MOSAIC chemistry without halogen chemistry resulted in an unrealistic ozone mixing ratio at Utqiaġvik, anti-correlating with observations and a strong bias for large ozone mixing ratios which demonstrates the impact of halogen chemistry on the prediction of ODEs.

BrO may be emitted by the extended bromine explosion mechanism and/or oxidation of bromide by ozone directly from the sea ice. The reactive surface ratio β accounts for non-flat surfaces such as snow/ice and controls the emission strength. Both simulations with standard emission (simulation 2, $\beta = 1.0$) and a simulation with enhanced emission (simulation 3), $\beta = 1.5$ perform with correlations to observations of more than 0.6 at Utqiaġvik for both vertical ozone profiles and BrO VCDs. Enhancing the emission strongly improves the mean bias, whereas correlation and RMSE only improved slightly with enhanced emissions, which is likely due to an overestimation of BrO emissions which occur more frequently. Generally, ozone depletion at Utqiaġvik is somewhat under-predicted by both simulations. ODEs identified by the model that are not present in the observations are rare: simulation 2 and 3 identify two and six ODEs, respectively. Simulation 2 finds half of the twenty-two observed ODEs whereas simulation 3 improves this prediction to more than two third of the observed ODEs.

https://doi.org/10.5194/acp-2020-952
Preprint. Discussion started: 13 November 2020


Atmospheric Chemistry and Physics Discussions

At Summit, the observations and simulations agree in identifying no ODEs. A tropopause fold is found by the simulations at the end of April 2009 in agreement with the observations.

At Utqiaġvik, temperature is slightly over-predicted and wind speed slightly under-predicted both of which may contribute to an under-prediction of ODEs. BrO VCDs are found to be consistent with satellite observations. However, an under-prediction of BrO VCDs over land and an over-prediction of BrO VCDs over FY ice is apparent. This is probably due the assumptions of the emission scheme in the model: Snow covering FY ice is assumed to have unlimited bromide content, resulting in an overestimation of BrO emissions, whereas snow over land has no halogen content, overestimating the removal of BrO. More realistic assumptions in a future study may improve the results.

The direct emission of bromine due to bromide oxidation by ozone is found to be very important since it provides an initial seed of bromine which then triggers the bromine explosion. Simulation 4 with deactivated bromide oxidation by ozone under sunlight strongly reduces Br_2 emissions even though the value of β has been set to 2.0. Therefore, simulation 4 is inferior to simulations 2 and 3 with a reduced overall prediction skill of ODEs. Even with a larger emission rate, the bromine explosion mechanism alone does not produce enough BrO to explain the observations which is likely due to a missing trigger of ODEs to provide the bromide oxidation by ozone. An alternative trigger of ODEs that may be worthwhile to study in future is the bromide oxidation by the hydroxyl radical.

Meteorological nudging is found to be very important. A simulation with enhanced emissions by 50% but disabled meteorological nudging (simulation 6) performs much worse compared to simulations 2 and 3. At Utqiaġvik, the prediction of meteorological variables such as temperature, for which the mean bias increased by a factor of three and the RMSE by a factor of two, becomes worse during the simulation, in particular, the second half of the simulation has a strong bias to larger temperatures and a poorer skill for predicting ozone. Simulations 2 and 3 with β equal to 1.0 and 1.5 respectively, are found to perform best where simulation 3 is somewhat superior to simulation 2 at the cost of an over-prediction of BrO at some times. It might be worthwhile to search for an optimal setting for β in a future study.

In a follow-up study it is planned to simulate ODEs in the year 2019 for which the new TROPOMI BrO VCDs with a high resolution of 5.5 km x 3.5 km are available. For this purpose, the grid resolution will be increased in order to allow for a comparison of the more refined observation data.

Code and data availability. The software code and data may be obtained from the corresponding author upon request.

Author contributions. MH performed the simulations and wrote the paper draft. HS contributed the observational data. TW provided additional scientific support. UP and EG devised the methodology and supervised the project and EG revised the manuscript.

Competing interests. The authors declare that they have no conflict of interest.

https://doi.org/10.5194/acp-2020-952
Preprint. Discussion started: 13 November 2020

Atmospheric Chemistry and Physics Discussions

Acknowledgements. The authors gratefully acknowledge funding by the Deutsche Forschungsgemeinschaft (DFG, German Research Foundation) – Projektnummer 85276297 and through HGS Math-Comp. The authors acknowledge support by the state of Baden-Württemberg through bwHPC and the German Research Foundation (DFG) through grant INST 35/1134-1 FUGG, allowing the authors to conduct simulations using the bwForCluster MLS&WISO Development. ERA-Interim data provided courtesy ECMWF. GOME-2 level-1 data have been provided by ESA/EUMETSAT. In-situ data for ozone at Utqiaġvik and Summit and meteorology at Utqiaġvik were obtained from the NOAA/ESRL Global Monitoring Division (https://www.esrl.noaa.gov/gmd/). Ozone vertical profiles were obtained from the NOAA Earth System Research Laboratory (ESRL,http://www.esrl.noaa.gov/gmd/obop/brw). OSI-403-c sea ice type data were obtained from EUMETSAT OSI SAF (http://www.osi-saf.org/?q=content/global-sea-ice-type-c).

https://doi.org/10.5194/acp-2020-952
Preprint. Discussion started: 13 November 2020

Atmospheric Chemistry and Physics Discussions

References

Aaboe, S., Breivik, L., Sørensen, A., Eastwood, S., and Lavergne, T.: Global Sea Ice Edge (OSI-402-c) and Type (OSI-403-c) ProductUser'sManual–v2. 2. TechnicalReportSAF, Tech. rep., OSI/CDOP2/MET-Norway/TEC/MA/205, EUMETSAT OSI SAF–Ocean and Sea Ice . . . , 2017.

Artiglia, L., Edebeli, J., Orlando, F., Chen, S., Lee, M.-T., Arroyo, P. C., Gilgen, A., Bartels-Rausch, T., Kleibert, A., Vazdar, M., et al.: A surface-stabilized ozonide triggers bromide oxidation at the aqueous solution-vapour interface, Nature Communications, 8, 700, 2017.

Atkinson, H. M., Huang, R.-J., Chance, R., Roscoe, H. K., Hughes, C., Davison, B., Schönhardt, A., Mahajan, A. S., Saiz-Lopez, A., Hoffmann, T., et al.: Iodine emissions from the sea ice of the Weddell Sea, Atmospheric Chemistry and Physics, 12, 11 229–11 244, 2012.

Atkinson, R., Baulch, D. L., Cox, R. A., Crowley, J. N., Hampson, R. F., Hynes, R. G., Jenkin, M. E., Rossi, M. J., and Troe, J.: Evaluated kinetic and photochemical data for atmospheric chemistry: Volume III - gas phase reactions of inorganic halogens, Atmospheric Chemistry and Physics, 7, 981–1191, https://doi.org/10.5194/acp-7-981-2007, https://www.atmos-chem-phys.net/7/981/2007/, 2007.

Barrie, L., Bottenheim, J., Schnell, R., Crutzen, P., and Rasmussen, R.: Ozone destruction and photochemical reactions at polar sunrise in the lower Arctic atmosphere, Nature, 334, 138, 1988.

Bottenheim, J., Gallant, A., and Brice, K.: Measurements of NOy species and O3 at 82 N latitude, Geophysical Research Letters, 13, 113–116, 1986.

Bottenheim, J., Netcheva, S., Morin, S., and Nghiem, S.: Ozone in the boundary layer air over the Arctic Ocean: measurements during the TARA transpolar drift 2006–2008, Atmospheric Chemistry and Physics, 9, 4545–4557, 2009.

Bromwich, D. H., Hines, K. M., and Bai, L.-S.: Development and testing of polar weather research and forecasting model: 2. Arctic Ocean, Journal of Geophysical Research: Atmospheres, 114, 2009.

Bromwich, D. H., Otieno, F. O., Hines, K. M., Manning, K. W., and Shilo, E.: Comprehensive evaluation of polar weather research and forecasting model performance in the Antarctic, Journal of Geophysical Research: Atmospheres, 118, 274–292, 2013.

Callies, J., Corpaccioli, E., Eisinger, M., Hahne, A., and Lefebvre, A.: GOME-2- Metop's second-generation sensor for operational ozone monitoring, ESA bulletin, 102, 28–36, 2000.

Cao, L., Sihler, H., Platt, U., and Gutheil, E.: Numerical analysis of the chemical kinetic mechanisms of ozone depletion and halogen release in the polar troposphere, Atmos. Chem. Phys, 14, 377, 2014.

Custard, K. D., Raso, A. R. W., Shepson, P. B., Staebler, R. M., and Pratt, K. A.: Production and Release of Molecular Bromine and Chlorine from the Arctic Coastal Snowpack, ACS Earth and Space Chemistry, 1, 142–151, https://doi.org/10.1021/acsearthspacechem.7b00014, https://doi.org/10.1021/acsearthspacechem.7b00014, 2017.

Dee, D. P., Uppala, S. M., Simmons, A. J., Berrisford, P., Poli, P., Kobayashi, S., Andrae, U., Balmaseda, M. A., Balsamo, G., Bauer, P., Bechtold, P., Beljaars, A. C. M., van de Berg, L., Bidlot, J., Bormann, N., Delsol, C., Dragani, R., Fuentes, M., Geer, A. J., Haimberger, L., Healy, S. B., Hersbach, H., Hólm, E. V., Isaksen, L., Kållberg, P., Köhler, M., Matricardi, M., McNally, A. P., Monge-Sanz, B. M., Morcrette, J.-J., Park, B.-K., Peubey, C., de Rosnay, P., Tavolato, C., Thépaut, J.-N., and Vitart, F.: The ERA-Interim reanalysis: configuration and performance of the data assimilation system, Quarterly Journal of the Royal Meteorological Society, 137, 553–597, https://doi.org/10.1002/qj.828, https://rmets.onlinelibrary.wiley.com/doi/abs/10.1002/qj.828, 2011.

Emmons, L. K., Walters, S., Hess, P. G., Lamarque, J.-F., Pfister, G. G., Fillmore, D., Granier, C., Guenther, A., Kinnison, D., Laepple, T., et al.: Description and evaluation of the Model for Ozone and Related chemical Tracers, version 4 (MOZART-4), Geoscientific Model Development, 3, 43–67, 2010a.

https://doi.org/10.5194/acp-2020-952
Preprint. Discussion started: 13 November 2020

Emmons, L. K., Walters, S., Hess, P. G., Lamarque, J.-F., Pfister, G. G., Fillmore, D., Granier, C., Guenther, A., Kinnison, D., Laepple, T., et al.: Description and evaluation of the Model for Ozone and Related chemical Tracers, version 4 (MOZART-4), 2010b.

Falk, S. and Sinnhuber, B.-M.: Polar boundary layer bromine explosion and ozone depletion events in the chemistry-climate model EMAC v2. 52: implementation and evaluation of AirSnow algorithm., Geoscientific Model Development, 11, 2018.

Fan, S.-M. and Jacob, D. J.: Surface ozone depletion in Arctic spring sustained by bromine reactions on aerosols, Nature, 359, 522, 1992.

Fickert, S., Adams, J. W., and Crowley, J. N.: Activation of Br2 and BrCl via uptake of HOBr onto aqueous salt solutions, Journal of Geophysical Research: Atmospheres, 104, 23 719–23 727, https://doi.org/10.1029/1999JD900359, https://agupubs.onlinelibrary.wiley.com/doi/abs/10.1029/1999JD900359, 1999.

Frieß, U., Hollwedel, J., König-Langlo, G., Wagner, T., and Platt, U.: Dynamics and chemistry of tropospheric bromine explosion events in the Antarctic coastal region, Journal of Geophysical Research: Atmospheres, 109, 2004.

Fuchs, N. and Sutugin, A.: High-dispersed aerosols, in: Topics in current aerosol research, p. 1, Elsevier, 1971.

Grebel, J. E., Pignatello, J. J., and Mitch, W. A.: Effect of halide ions and carbonates on organic contaminant degradation by hydroxyl radical-based advanced oxidation processes in saline waters, Environmental science & technology, 44, 6822–6828, 2010.

Grell, G. A.: Prognostic Evaluation of Assumptions Used by Cumulus Parameterizations, Monthly Weather Review, 121, 764–787, https://doi.org/10.1175/1520-0493(1993)121<0764:PEOAUB>2.0.CO;2, https://doi.org/10.1175/1520-0493(1993)121<0764:PEOAUB>2.0.CO;2, 1993.

Grell, G. A., Peckham, S. E., Schmitz, R., McKeen, S. A., Frost, G., Skamarock, W. C., and Eder, B.: Fully coupled "online" chemistry within the WRF model, Atmospheric Environment, 39, 6957–6975, 2005.

Guenther, A., Karl, T., Harley, P., Wiedinmyer, C., Palmer, P. I., and Geron, C.: Estimates of global terrestrial isoprene emissions using MEGAN (Model of Emissions of Gases and Aerosols from Nature), Atmospheric Chemistry and Physics, 6, 3181–3210, https://hal.archives-ouvertes.fr/hal-00295995, 2006.

Halfacre, J. W., Knepp, T. N., Shepson, P. B., Thompson, C. R., Pratt, K. A., Li, B., Peterson, P. K., Walsh, S. J., Simpson, W. R., Matrai, P. A., Bottenheim, J. W., Netcheva, S., Perovich, D. K., and Richter, A.: Temporal and spatial characteristics of ozone depletion events from measurements in the Arctic, Atmospheric Chemistry and Physics, 14, 4875–4894, https://doi.org/10.5194/acp-14-4875-2014, https://www.atmos-chem-phys.net/14/4875/2014/, 2014.

Halfacre, J. W., Shepson, P. B., and Pratt, K. A.: pH-dependent production of molecular chlorine, bromine, and iodine from frozen saline surfaces, Atmospheric Chemistry and Physics, 19, 4917–4931, https://doi.org/10.5194/acp-19-4917-2019, https://acp.copernicus.org/articles/19/4917/2019/, 2019.

Hausmann, M. and Platt, U.: Spectroscopic measurement of bromine oxide and ozone in the high Arctic during Polar Sunrise Experiment 1992, Journal of Geophysical Research: Atmospheres, 99, 25 399–25 413, 1994.

Helmig, D., Boylan, P., Johnson, B., Oltmans, S., Fairall, C., Staebler, R., Weinheimer, A., Orlando, J., Knapp, D. J., Montzka, D. D., et al.: Ozone dynamics and snow-atmosphere exchanges during ozone depletion events at Barrow, Alaska, Journal of Geophysical Research: Atmospheres, 117, 2012.

Herrmann, M., Cao, L., Sihler, H., Platt, U., and Gutheil, E.: On the contribution of chemical oscillations to ozone depletion events in the polar spring, Atmospheric Chemistry and Physics, 19, 10 161–10 190, https://doi.org/10.5194/acp-19-10161-2019, https://www.atmos-chem-phys.net/19/10161/2019/, 2019.

Hong, S.-Y. and Lim, J.-O. J.: The WRF single-moment 6-class microphysics scheme (WSM6), Asia-Pacific Journal of Atmospheric Sciences, 42, 129–151, 2006.

https://doi.org/10.5194/acp-2020-952
Preprint. Discussion started: 13 November 2020


Atmospheric Chemistry and Physics Discussions

Iacono, M. J., Delamere, J. S., Mlawer, E. J., Shephard, M. W., Clough, S. A., and Collins, W. D.: Radiative forcing by long-lived greenhouse gases: Calculations with the AER radiative transfer models, Journal of Geophysical Research: Atmospheres, 113, https://doi.org/10.1029/2008JD009944, https://agupubs.onlinelibrary.wiley.com/doi/abs/10.1029/2008JD009944, 2008.

Janjić, Z.: The surface layer in the NCEP Eta Model, in: Eleventh Conference on Numerical Weather Prediction, pp. 19–23, Amer. Meteor. Soc. Norfolk, VA, 1996.

Janjić, Z. I.: The step-mountain coordinate: Physical package, Monthly Weather Review, 118, 1429–1443, 1990.

Janssens-Maenhout, G., Dentener, F., Van Aardenne, J., Monni, S., Pagliari, V., Orlandini, L., Klimont, Z., Kurokawa, J.-i., Akimoto, H., Ohara, T., et al.: EDGAR-HTAP: a harmonized gridded air pollution emission dataset based on national inventories, European Commission Publications Office, Ispra (Italy). JRC68434, EUR report No EUR, 25, 299–2012, 2012.

Johnson, B. J., Oltmans, S. J., and Booth, J.: Boundary Layer Ozone Depletion Events Measured by Ozonesondes at Barrow, Alaska in 2009, in: AGU Fall Meeting Abstracts, vol. 2009, pp. A31C–0108, 2009.

Kaleschke, L., Richter, A., Burrows, J., Afe, O., Heygster, G., Notholt, J., Rankin, A., Roscoe, H., Hollwedel, J., Wagner, T., et al.: Frost flowers on sea ice as a source of sea salt and their influence on tropospheric halogen chemistry, Geophysical research letters, 31, 2004.

Koo, J.-H., Wang, Y., Kurosu, T., Chance, K., Rozanov, A., Richter, A., Oltmans, S., Thompson, A., Hair, J., Fenn, M., et al.: Characteristics of tropospheric ozone depletion events in the Arctic spring: analysis of the ARCTAS, ARCPAC, and ARCIONS measurements and satellite BrO observations, Atmospheric Chemistry and Physics, 12, 9909–9922, 2012.

Lehrer, E., Hönninger, G., and Platt, U.: A one dimensional model study of the mechanism of halogen liberation and vertical transport in the polar troposphere, Atmos. Chem. Phys., 4, 2427–2440, 2004.

Luther, G. W., Swartz, C. B., and Ullman, W. J.: Direct determination of iodide in seawater by cathodic stripping square wave voltammetry, Analytical Chemistry, 60, 1721–1724, 1988.

Madronich, S., Flocke, S., Zeng, J., Petropavlovskikh, I., and Lee-Taylor, J.: Tropospheric Ultraviolet-Visible Model (TUV) version 4.1, National Center for Atmospheric Research, PO Box, 3000, 2002.

McClure-Begley, A., Petropavlovskikh, I., and Oltmans, S.: NOAA Global Monitoring Surface Ozone Network, 1973–2014, National Oceanic and Atmospheric Administration, Earth Systems Research Laboratory Global Monitoring Division, Boulder, CO, doi, 10, V57P8WBF, 2014.

McConnell, J., Henderson, G., Barrie, L., Bottenheim, J., Niki, H., Langford, C., and Templeton, E.: Photochemical bromine production implicated in Arctic boundary-layer ozone depletion, Nature, 355, 150, 1992.

McNamara, S. M., Garner, N. M., Wang, S., Raso, A. R. W., Thanekar, S., Barget, A. J., Fuentes, J. D., Shepson, P. B., and Pratt, K. A.: Bromine Chloride in the Coastal Arctic: Diel Patterns and Production Mechanisms, ACS Earth and Space Chemistry, 4, 620–630, https://doi.org/10.1021/acsearthspacechem.0c00021, https://doi.org/10.1021/acsearthspacechem.0c00021, 2020.

Mefford, T., Bieniulis, M., Halter, B., and Peterson, J.: Meteorological Measurements, CMDL Summary Report, 1995, 1994.

Mellor, G. L. and Yamada, T.: Development of a turbulence closure model for geophysical fluid problems, Reviews of Geophysics, 20, 851–875, 1982.

Munro, R., Eisinger, M., Anderson, C., Callies, J., Corpaccioli, E., Lang, R., Lefebvre, A., Livschitz, Y., and Albinana, A. P.: GOME-2 on MetOp, in: Proc. of The 2006 EUMETSAT Meteorological Satellite Conference, Helsinki, Finland, vol. 12–16 June 2006, ISBN 92-9110-076-5, EUMETSAT, p. 48, 2006.

https://doi.org/10.5194/acp-2020-952
Preprint. Discussion started: 13 November 2020

Nasse, J.-M., Eger, P. G., Pöhler, D., Schmitt, S., Frieß, U., and Platt, U.: Recent improvements of long-path DOAS measurements: impact on accuracy and stability of short-term and automated long-term observations, Atmospheric Measurement Techniques, 12, 4149–4169, 2019.

Niu, G.-Y., Yang, Z.-L., Mitchell, K. E., Chen, F., Ek, M. B., Barlage, M., Kumar, A., Manning, K., Niyogi, D., Rosero, E., et al.: The community Noah land surface model with multiparameterization options (Noah-MP): 1. Model description and evaluation with local-scale measurements, Journal of Geophysical Research: Atmospheres, 116, 2011.

Oltmans, S.: Surface ozone measurements in clean air, Journal of Geophysical Research: Oceans, 86, 1174–1180, https://doi.org/10.1029/JC086iC02p01174, https://agupubs.onlinelibrary.wiley.com/doi/abs/10.1029/JC086iC02p01174, 1981.

Oltmans, S. J., Johnson, B. J., and Harris, J. M.: Springtime boundary layer ozone depletion at Barrow, Alaska: Meteorological influence, year-to-year variation, and long-term change, Journal of Geophysical Research: Atmospheres, 117, https://doi.org/https://doi.org/10.1029/2011JD016889, https://agupubs.onlinelibrary.wiley.com/doi/abs/10.1029/2011JD016889, 2012.

Oum, K., Lakin, M., and Finlayson-Pitts, B.: Bromine activation in the troposphere by the dark reaction of O3 with seawater ice, Geophysical Research Letters, 25, 3923–3926, 1998.

Peaceman, D. W. and Rachford, Jr, H. H.: The numerical solution of parabolic and elliptic differential equations, Journal of the Society for industrial and Applied Mathematics, 3, 28–41, 1955.

Peterson, P. K., Pöhler, D., Zielcke, J., General, S., Frieß, U., Platt, U., Simpson, W. R., Nghiem, S. V., Shepson, P. B., Stirm, B. H., and Pratt, K. A.: Springtime Bromine Activation over Coastal and Inland Arctic Snowpacks, ACS Earth and Space Chemistry, 2, 1075–1086, https://doi.org/10.1021/acsearthspacechem.8b00083, https://doi.org/10.1021/acsearthspacechem.8b00083, 2018.

Peterson, P. K., Hartwig, M., May, N. W., Schwartz, E., Rigor, I., Ermold, W., Steele, M., Morison, J. H., Nghiem, S. V., and Pratt, K. A.: Snowpack measurements suggest role for multi-year sea ice regions in Arctic atmospheric bromine and chlorine chemistry, Elementa (Washington, DC), 7, 2019.

Platt, U. and Janssen, C.: Observation and role of the free radicals NO 3, ClO, BrO and IO in the troposphere, Faraday Discussions, 100, 175–198, 1995.

Platt, U. and Lehrer, E.: Arctic tropospheric ozone chemistry, ARCTOC, no. 64 in Air pollution research report, European Commission Directorate-General, Science, Research and Development, Luxembourg, 1997.

Pöhler, D., Vogel, L., Frieß, U., and Platt, U.: Observation of halogen species in the Amundsen Gulf, Arctic, by active long-path differential optical absorption spectroscopy, Proceedings of the National Academy of Sciences, 107, 6582–6587, 2010.

Pratt, K. A., Custard, K. D., Shepson, P. B., Douglas, T. A., Pöhler, D., General, S., Zielcke, J., Simpson, W. R., Platt, U., Tanner, D. J., et al.: Photochemical production of molecular bromine in Arctic surface snowpacks, Nature Geoscience, 6, 351, 2013.

Raso, A. R., Custard, K. D., May, N. W., Tanner, D., Newburn, M. K., Walker, L., Moore, R. J., Huey, L. G., Alexander, L., Shepson, P. B., et al.: Active molecular iodine photochemistry in the Arctic, Proceedings of the National Academy of Sciences, 114, 10 053–10 058, 2017.

Saiz-Lopez, A., Mahajan, A. S., Salmon, R. A., Bauguitte, S. J.-B., Jones, A. E., Roscoe, H. K., and Plane, J. M.: Boundary layer halogens in coastal Antarctica, Science, 317, 348–351, 2007.

Sander, R., Baumgaertner, A., Gromov, S., Harder, H., Jöckel, P., Kerkweg, A., Kubistin, D., Regelin, E., Riede, H., Sandu, A., Taraborrelli, D., Tost, H., and Xie, Z.-Q.: The atmospheric chemistry box model CAABA/MECCA-3.0, Geoscientific Model Development, 4, 373–380, https://doi.org/10.5194/gmd-4-373-2011, https://www.geosci-model-dev.net/4/373/2011/, 2011.

Sihler, H., Platt, U., Beirle, S., Marbach, T., Kühl, S., Dörner, S., Verschaeve, J., Frieß, U., Pöhler, D., Vogel, L., Sander, R., and Wagner, T.: Tropospheric BrO column densities in the Arctic derived from satellite: retrieval and comparison to ground-based measurements, At-

mospheric Measurement Techniques, 5, 2779–2807, https://doi.org/10.5194/amt-5-2779-2012, https://www.atmos-meas-tech.net/5/2779/2012/, 2012.

Simpson, W., Glasow, R. v., Riedel, K., Anderson, P., Ariya, P., Bottenheim, J., Burrows, J., Carpenter, L., Frieß, U., Goodsite, M. E., et al.: Halogens and their role in polar boundary-layer ozone depletion, Atmospheric Chemistry and Physics, 7, 4375–4418, 2007a.

Simpson, W. R., Alvarez-Aviles, L., Douglas, T. A., Sturm, M., and Domine, F.: Halogens in the coastal snow pack near Barrow, Alaska: Evidence for active bromine air-snow chemistry during springtime, Geophysical research letters, 32, 2005.

Simpson, W. R., Carlson, D., Hönninger, G., Douglas, T. A., Sturm, M., Perovich, D., and Platt, U.: First-year sea-ice contact predicts bromine monoxide (BrO) levels at Barrow, Alaska better than potential frost flower contact, Atmospheric Chemistry and Physics, 7, 621–627, https://doi.org/10.5194/acp-7-621-2007, https://www.atmos-chem-phys.net/7/621/2007/, 2007b.

Simpson, W. R., Brown, S. S., Saiz-Lopez, A., Thornton, J. A., and von Glasow, R.: Tropospheric halogen chemistry: Sources, cycling, and impacts, Chemical reviews, 115, 4035–4062, 2015.

Sjostedt, S. J. and Abbatt, J. P. D.: Release of gas-phase halogens from sodium halide substrates: heterogeneous oxidation of frozen solutions and desiccated salts by hydroxyl radicals, Environmental Research Letters, 3, 045 007, https://doi.org/10.1088/1748-9326/3/4/045007, https://doi.org/10.1088%2F1748-9326%2F3%2F4%2F045007, 2008.

Skamarock, W. C., Klemp, J. B., Dudhia, J., Gill, D. O., Barker, D. M., Wang, W., and Powers, J. G.: A description of the Advanced Research WRF version 3. NCAR Technical note-475+ STR, https://doi.org/10.5065/D68S4MVH, 2008.

Tarasick, D. and Bottenheim, J.: Surface ozone depletion episodes in the Arctic and Antarctic from historical ozonesonde records, Atmospheric Chemistry and Physics, 2, 197–205, 2002.

Thiébaux, J., Rogers, E., Wang, W., and Katz, B.: A New High-Resolution Blended Real-Time Global Sea Surface Temperature Analysis, Bulletin of the American Meteorological Society, 84, 645–656, https://doi.org/10.1175/BAMS-84-5-645, https://doi.org/10.1175/BAMS-84-5-645, 2003.

Thomas, J. L., Stutz, J., Lefer, B., Huey, L. G., Toyota, K., Dibb, J. E., and von Glasow, R.: Modeling chemistry in and above snow at Summit, Greenland – Part 1: Model description and results, Atmospheric Chemistry and Physics, 11, 4899–4914, https://doi.org/10.5194/acp-11-4899-2011, https://acp.copernicus.org/articles/11/4899/2011/, 2011.

Toyota, K., McConnell, J. C., Lupu, A., Neary, L., McLinden, C. A., Richter, A., Kwok, R., Semeniuk, K., Kaminski, J. W., Gong, S.-L., Jarosz, J., Chipperfield, M. P., and Sioris, C. E.: Analysis of reactive bromine production and ozone depletion in the Arctic boundary layer using 3-D simulations with GEM-AQ: inference from synoptic-scale patterns, Atmospheric Chemistry and Physics, 11, 3949–3979, https://doi.org/10.5194/acp-11-3949-2011, https://www.atmos-chem-phys.net/11/3949/2011/, 2011.

Toyota, K., McConnell, J. C., Staebler, R. M., and Dastoor, A. P.: Air–snowpack exchange of bromine, ozone and mercury in the springtime Arctic simulated by the 1-D model PHANTAS - Part 1: In-snow bromine activation and its impact on ozone, Atmospheric Chemistry and Physics, 14, 4101–4133, https://doi.org/10.5194/acp-14-4101-2014, https://www.atmos-chem-phys.net/14/4101/2014/, 2014.

Wagner, T. and Platt, U.: Satellite mapping of enhanced BrO concentrations in the troposphere, Nature, 395, 486–490, 1998.

Wagner, T., Leue, C., Wenig, M., Pfeilsticker, K., and Platt, U.: Spatial and temporal distribution of enhanced boundary layer BrO concentrations measured by the GOME instrument aboard ERS-2, Journal of Geophysical Research: Atmospheres, 106, 24 225–24 235, 2001.

Wagner, T., Ibrahim, O., Sinreich, R., Frieß, U., von Glasow, R., and Platt, U.: Enhanced tropospheric BrO over Antarctic sea ice in mid winter observed by MAX-DOAS on board the research vessel Polarstern, Atmospheric Chemistry and Physics, 7, 3129–3142, https://doi.org/10.5194/acp-7-3129-2007, https://www.atmos-chem-phys.net/7/3129/2007/, 2007.

https://doi.org/10.5194/acp-2020-952
Preprint. Discussion started: 13 November 2020

Wang, S. and Pratt, K. A.: Molecular Halogens Above the Arctic Snowpack: Emissions, Diurnal Variations, and Recycling Mechanisms, Journal of Geophysical Research: Atmospheres, 122, 11,991–12,007, https://doi.org/https://doi.org/10.1002/2017JD027175, https://agupubs.onlinelibrary.wiley.com/doi/abs/10.1002/2017JD027175, 2017.

Wang, S., McNamara, S. M., Moore, C. W., Obrist, D., Steffen, A., Shepson, P. B., Staebler, R. M., Raso, A. R. W., and Pratt, K. A.: Direct detection of atmospheric atomic bromine leading to mercury and ozone depletion, Proceedings of the National Academy of Sciences, 116, 14 479–14 484, https://doi.org/10.1073/pnas.1900613116, https://www.pnas.org/content/116/29/14479, 2019.

Wennberg, P.: Atmospheric chemistry: Bromine explosion, Nature, 397, 299, 1999.

Wesely, M.: Parameterization of surface resistances to gaseous dry deposition in regional-scale numerical models, Atmospheric Environment (1967), 23, 1293–1304, 1989.

Wexler, A. S. and Seinfeld, J. H.: Second-generation inorganic aerosol model, Atmospheric Environment. Part A. General Topics, 25, 2731–2748, 1991.

Wilson, A. B., Bromwich, D. H., and Hines, K. M.: Evaluation of Polar WRF forecasts on the Arctic System Reanalysis domain: Surface and upper air analysis, Journal of Geophysical Research: Atmospheres, 116, 2011.

Wren, S. N. and Donaldson, D. J.: How does deposition of gas phase species affect pH at frozen salty interfaces?, Atmospheric Chemistry and Physics, 12, 10 065–10 073, https://doi.org/10.5194/acp-12-10065-2012, https://acp.copernicus.org/articles/12/10065/2012/, 2012.

Yang, X., Pyle, J. A., and Cox, R. A.: Sea salt aerosol production and bromine release: Role of snow on sea ice, Geophysical Research Letters, 35, n/a–n/a, https://doi.org/10.1029/2008GL034536, http://dx.doi.org/10.1029/2008GL034536, l16815, 2008.

Yang, X., Pyle, J. A., Cox, R. A., Theys, N., and Van Roozendael, M.: Snow-sourced bromine and its implications for polar tropospheric ozone, Atmospheric Chemistry and Physics, 10, 7763–7773, https://doi.org/10.5194/acp-10-7763-2010, https://www.atmos-chem-phys.net/10/7763/2010/, 2010.

Zaveri, R. A., Easter, R. C., Fast, J. D., and Peters, L. K.: Model for simulating aerosol interactions and chemistry (MOSAIC), Journal of Geophysical Research: Atmospheres, 113, 2008.

Zhao, T. L., Gong, S. L., Bottenheim, J. W., McConnell, J. C., Sander, R., Kaleschke, L., Richter, A., Kerkweg, A., Toyota, K., and Barrie, L. A.: A three-dimensional model study on the production of BrO and Arctic boundary layer ozone depletion, Journal of Geophysical Research: Atmospheres, 113, https://doi.org/10.1029/2008JD010631, https://agupubs.onlinelibrary.wiley.com/doi/abs/10.1029/2008JD010631, 2008.

Zielcke, J.: Observations of reactive bromine, iodine and chlorine species in the Arctic and Antarctic with differential optical absorption spectroscopy, Ph.D. thesis, (Ruperto-Carola University, Heidelberg, 2015.